

University Degree in Aerospace Engineering
September 2018

Bachelor Thesis

A Parametric Modal Decomposition for Fluid Mechanics Problems

Daniel Rubio García

Tutor

Marco Raiola



Abstract

Modal decomposition is widely used to simplify complex fluid mechanics problems by splitting the data set of the problem into different modes, which collect the main effects of the parameters involved in the problem. This data set is collected in a matrix form. Nevertheless, in case of the presence of more than two parameters affecting the system, a tensor multilinear modal decomposition should be applied.

In this thesis, a brief development of matrix and tensor decomposition is addressed. In addition, multilinear modal decomposition is applied to perform a parametric study of an experimental flapping wing problem, where a large number of parameters can influence the system.

Finally, it is obtained that the multilinear modal decomposition is a powerful method to simplify and extract the most significant features of a system. Since this method is only an experimental and mathematical method, it allows to extract the most relevant behaviors of each parameter without the necessity of entering into too much detail in the field of fluid mechanics.

Keywords: modal decomposition, N-way principal component analysis, multilinear singular value decomposition, flapping wings

L^AT_EX was used as text editor.

Matlab 2017a was used as programming tool.

TensorLab package [1] was used to work with tensors.

Acknowledgements

I would like to thank Marco Raiola for being so patient with me and for the never ending tutoring sessions.

To my colleagues Juan, Dani, Adrián, Diego and Manu for helping me and having so much fun with you during these last four years.

Last but not least, I would like to thank my parents and brothers for their support in the most difficult times in my life.

Thank you.

Contents

	Page
1 Introduction	1
1.1 Motivation	1
1.2 Socio-economic impact of the project	2
1.3 Regulatory framework	2
1.4 Budget	3
1.5 Outline	3
2 State of the art	5
2.1 Matrix Decomposition	5
2.1.1 Eigenvalue Decomposition	5
2.1.2 Singular Value Decomposition (SVD)	5
2.1.3 Proper Orthogonal Decomposition (POD)	6
2.2 Tensor Decomposition	7
3 Mathematical background	9
3.1 Notation	9
3.2 Eigenvalue Decomposition	9
3.3 Singular Value Decomposition (SVD)	10
3.4 Proper Orthogonal Decomposition (POD)	11
3.4.1 Classical POD Method	11
3.4.2 Method of Snapshots	12
3.4.3 SVD and POD	12
3.5 Preliminary concepts of tensor calculus	13
3.5.1 Subtensors and fibers of a tensor	13
3.5.2 Matricization	14
3.5.3 Matrix Kronecker product	16
3.5.4 Khatri-Rao product	17
3.5.5 Multiplication of a tensor by a matrix: n -mode product	17
3.6 Multilinear Singular Value Decomposition (MLSVD)	18
3.6.1 The n -rank	19
3.7 CP Decomposition	21
3.8 Matlab matrix notation	23
4 Flapping wings parametric study	25
4.1 Introduction of flapping wings	25

4.2	Objective of the study	28
4.3	Experimental data set details	29
4.3.1	Data collection	29
4.3.2	Sources of error	30
4.3.3	C_L and C_D rotation	31
4.3.4	Tensor construction	32
5	Results	33
5.1	Parametric study of C_Y	33
5.2	Parametric study of C_X	42
6	Discussion and summary	49
6.1	Effect of pitching amplitude θ_0 and mean pitch angle θ_m	49
6.2	Effect of the <i>Strouhal number</i>	50
6.3	Summary	51
7	Future work	53
	References	55

List of Figures

1	Illustration of the first mode (blue) and second mode (red). Adopted from [34].	13
2	Subtensors of a 3^{rd} order tensor. Adopted from [33].	13
3	Fibers of a 3^{rd} order tensor. Adopted from [33].	14
4	Matricization of a $I_1 \times I_2 \times I_3$ tensor. Adopted from [19].	15
5	Visualization of a Tucker decomposition of a 3D tensor \mathcal{A} . Adopted from [33].	18
6	Truncated Tucker Decomposition. Adopted from [33].	20
7	Illustration of the CP decomposition. Adopted from [33].	22
8	Plunge motion. Adopted from [2].	26
9	Pitch motion. Adopted from [2].	26
10	Airfoil trajectory combining heave motion and a 180° pitch change. Adopted from [39].	26
11	Scheme of the rotation of C_L and C_D	31
12	33
13	(a) θ_0 effect on C_Y with $\theta_m = 0^\circ$ and $St = 0.3$; (b) θ_m effect on C_Y with $\theta_0 = 5^\circ$ and $St = 0.3$; (c) St effect on C_Y with $\theta_0 = 0^\circ$ and $\theta_m = 0^\circ$. 36	
14	Most relevant modes of \mathcal{C}_Y	37
15	(a) C_Y variation with θ_0 ($\theta_m = 0^\circ$ and $St = 0.2$) and the reconstruction using just the most relevant mode combination; (b) C_Y variation with St ($\theta_0 = 0^\circ$ and $\theta_m = 0^\circ$). Reconstruction cases are depicted in dotted lines.	38
16	(a) Reconstruction of $C_Y(2, :, 2, 2)$; (b) Reconstruction of $C_Y(1, :, 1, 1)$; (c) Reconstruction of $C_Y(1, :, 2, 1)$	41
17	(a) θ_0 effect on C_X with $\theta_m = 0^\circ$ and $St = 0.1$; (b) θ_m effect on C_X with $\theta_0 = 5^\circ$ and $St = 0.1$; (c) St effect on C_X with $\theta_0 = 5^\circ$ and $\theta_m = 5^\circ$. 43	
18	Most important modes combination of \mathcal{C}_X	44
19	(a) Reconstruction of $C_X(3, :, 3, 3)$; (b) $C_X(1, :, 1, 2)$; (c) $C_X(1, :, 1, 1)$ with n mode combinations.	46
20	Variation of the effective angle of attack (α_{eff}) with θ_0 (a) and θ_m (b). Adopted from [2].	50

List of Tables

1	Values of parameters	30
2	Coefficient letter corresponding to each parameter.	32
3	Leading mode combinations of C_Y according to the <i>comparison method</i>	35
4	Coefficient of determination as function of time cases and number of mode combinations.	40
5	Leading mode combinations of C_X according to the <i>comparison method</i>	42
6	Coefficient of determination as function of time cases and number of mode combinations.	45
7	Summary of the effect of each parameter on the amplitude of C_Y and C_X according to the modal decomposition results.	49

1 Introduction

1.1 Motivation

Fluid mechanics problems are very complex to understand and they are tried to be solved using complex physical models which need a large amount of resources. However, there is one method that could be able to extract the most relevant information of a system without the use of such complex models. This method is called *modal decomposition*. Modal decomposition is a mathematical procedure that can be used to extract the most energetic features of a flow field. There are two types of modal decompositions: the analytical and the data-driven modal decomposition. The analytical consists on the extraction of the modes parting from the equations that govern the system. In case of fluid mechanics, those equations are usually the Navier-Stokes equations. On the other hand, the data-driven procedure is based on the matrix decomposition of the data set coming from either numerical simulations or experimental data. The experimental method could be able to extract reliable information of the system without the necessity of entering into detail inside the complex equations that govern the problem. This thesis is based on the experimental procedure.

Modal decomposition for two variables has been already applied to fluid mechanics problems, e.g. using the Singular Value Decomposition (SVD) for an experimental data set. The data-driven modal decomposition in fluid mechanics is called *Proper Orthogonal Decomposition* (POD).

Regarding the fluid mechanics field, the POD has been widely used to study velocity fields which only implies two variables: space and time. However, the modal decomposition for the case of more than two variables has remained untouched. In this way, a multilinear modal decomposition can be used to study the effect of more than two parameters on a fluid mechanics problem without the necessity of entering into too much detail in the field studied.

1.2 Socio-economic impact of the project

A multilinear modal decomposition could significantly simplify complex problems not only on the fluid mechanics field but on any other field involving a large number of variables like structural analysis, chemometrics, or even fields not related to engineering tasks such as sociology, economics or biology.

This modal decomposition allows to extract the most relevant behaviors of each parameter affecting the system without the necessity of entering into too much detail in the field studied.

Summarizing, this method could allow to accelerate the process of understanding complex problems without fully understand the natural laws behind that problem at a first insight.

1.3 Regulatory framework

As the studied topic is a purely theoretical work applied to a fluid mechanics problem, there is not a clear defined legislation about this topic. However, this modal decomposition can be used in other fields like statistics applicable to sociology. In a sociological study, the privacy policy plays an important role nowadays. The most recent privacy policy was the so-called GDPR (General Data Protection Regulation) approved by the European Union in 2016 and become effective in 25th May 2018.

On the other hand, the topic of flapping wings has not a defined regulation yet. However, flapping wings can be used as propulsive system of micro-air vehicles (MAVs). MAVs, together with bigger drones, are regulated in Spain by the *Real Decreto 1036/2017*. In addition, Unmanned Aerial Vehicles (UAVs) are currently on the core of discussion for the cooperation between Unmanned Traffic Management (UTM) and Air Traffic Management (ATM).

1.4 Budget

The first element of the budget would be the personnel costs. The time employed in this project was around 360 hours. Taking into account that the salary of a junior engineer in Spain is 10 €/hour, the total personnel cost is 3,600 €.

The last elements accounting for the budget are the resources used for the development of the project. In this instance, only Matlab has been used to perform the required calculations. The Matlab annual license costs 800 €.

Moreover, it should be added the cost of the experiment carried out by Carrillo [2] from which the data is collected. However, the costs of that experiment is out of scope for the budget of this project.

Summing up all the mentioned costs, the budget of this project is 4,400 €.

1.5 Outline

The rest of the thesis is organized as follows. In Section 2, the state of the art of modal decomposition from a theoretical point of view is developed. In Section 3, all the mathematical background around the modal decomposition for matrices and tensors is briefly explained. In addition, Section 4 tackles the application of modal decomposition in a flapping wing problem. First, a brief introduction of flapping wings topic is addressed followed by the explanation of some details about the experiment from which the data has been taken. Then, in Section 5 the results obtained by the modal decomposition are presented while in Section 6, these results are discussed from a literature point of view. Finally, Section 7 concludes with a couple of ideas of future work about this topic.

2 State of the art

This section presents the current state of the art of matrix and tensor decomposition as well as some of its applications. In addition, the most important decomposition methods are assessed such as the eigenvalue decomposition, the SVD, the POD, the PCA as well as tensor decomposition methods like the MLSVD and the CP decomposition.

2.1 Matrix Decomposition

Matrices are used to collect and interpret a two-dimensional data set. Matrix decomposition tries to split a matrix into several meaningful parts in order to seek out the most relevant terms and interpret them.

2.1.1 Eigenvalue Decomposition

The first and most basic matrix decomposition is the *eigenvalue decomposition*, also called *spectral decomposition*. Eigenvalues and eigenvectors of a matrix show the direction and magnitude of the column vectors of the matrix. However, the main limitation of this method is that it is only applicable to squares matrices. The eigenvalue decomposition is used in a lot of applications such as differential equations or vibration analysis but the most important application is that this decomposition is the foundations of the following decomposition methods of the present work like the SVD.

2.1.2 Singular Value Decomposition (SVD)

On the contrary of the eigenvalue decomposition, the SVD is not limited to square matrices and always exists. This is the reason of being the most important matrix factorization, that improves and expands the eigenvalue decomposition. The main idea of SVD is to find a set of orthonormal vectors in a subspace. In the present day, SVD is used in a wide variety of fields. The most basic use of SVD is to solve m simultaneous linear equations $\mathbf{M}\mathbf{x} = \mathbf{b}$ in a very efficient way. In addition, singular decompositions have shown its value in expressing the theory of *least squares* in a simpler way [3]. Most recently, SVD has been used for the dimensionality reduction of the data as well as for the extraction of weak signals from noisy data. The

ability of dimensionality reduction has been used, for instance, in image processing and compression. SVD allows a simple way of reducing the rank of the matrix by removing the smallest singular values (see Section 3.3). In this way, not only compression of the image is achieved but also a considerable noise reduction. Taking advantage of the noise reduction property of the SVD, Freire & Ulrych [4] applied this method to vertical seismic profiles (VSP) where they were able to isolate the uncorrelated noise. Furthermore, SVD is used in applications that involves a large amount of data such as chemometrics [5], molecular dynamics [6] or gene expression analysis [7].

2.1.3 Proper Orthogonal Decomposition (POD)

While SVD is a purely mathematical method, POD uses the theory of SVD to extract physical information. POD, also known as *Karhunen-Loève expansion* or *Principal Component Analysis* (PCA), is a modal decomposition used to extract the modes based on optimizing the mean square of the data set analyzed. In other words, POD allows to extract coherent physical structures from a large data set apparently random and uncorrelated. This coherent structures are called *modes* and correspond to the vector columns of the side matrices obtained with the SVD.

POD was first introduced by Lumley in 1967 [8] in order to better study turbulent flows. Later, in 1987, Sirovich [9] developed the *snapshot method* as a way to obtain the POD modes efficiently in problems involving a large amount of data.

POD has been used to obtain dominant features from data sets in a wide variety of fields like turbulent flows [10] or structural vibration analysis [11]. Additionally, Bernero & Fiedler [12] used a combination of POD and Particle Image Velocimetry (PIV) to isolate typical patterns from an apparently chaotic fluctuations of the counterflow of a jet. An unusual POD application was developed by Bui et al. [13], who used a "gappy" POD method in order to reconstruct incomplete or inaccurate aerodynamic data. They found that this procedure is not only effective to reconstruct data but to have a simple and effective approach to the inverse design of airfoil shapes.

Although POD has been widely used to capture the time variation of fluid mechanics problems, the use in parametric studies has been less common. For instance, Epureanu et al. [14] used the POD to develop models for turbomachinery flows with sampling in both time and over a range of interblade phase angles. In addition, Ly & Tran [15] used the POD to predict the steady-state temperature distribution of

a flow in a square cavity as the Rayleigh number is varied. The method used was a simple combination of POD and an interpolation.

Another examples of the applications of PCA include image processing, data compression and visualization, time series prediction and pattern recognition.

2.2 Tensor Decomposition

Matrix modal decomposition can be only applied to a two-dimensional data set. Nevertheless, it is often desirable to have a more global vision of a problem and take into account more than two variables to perform a parametric study. In case of multivariable data, analyzing a data set as a loose collection of isolated matrices leads to loss of information about correlations between parameters. Therefore, multivariable data should be stored in *multidimensional arrays*, also called *tensors*. An N^{th} order tensor is composed by N number of variables.

During the last decades, there has been a fast development of the mathematics and implementation of efficient algorithms about tensor decomposition thanks to its applications in a wide variety of fields involving large data sets like chemometrics, signal and imaging processing, bioinformatics or pattern recognition [16].

In the literature, there exist several ways of decomposing a higher-order tensor, being the two most relevant procedures the CP decomposition and the HOSVD.

The method of decomposing a higher-order tensor was first introduced by Tucker & Messick in 1963 [17] and improved until the so-called *Tucker3 Decomposition* [18]. In the literature, *Tucker3* is also called *Multilinear Singular Value Decomposition* (MLSVD), *Higher-Order Singular Value Decomposition* (HOSVD) [19] or *N-way Principal Component Analysis (N-way PCA)* [20]. The aim of the *Tucker3 Decomposition* is to represent the multivariable data set as a linear combination of few orthogonal factors called *modes*, similarly to the POD modes.

Polyadic form, this is, decomposing a tensor as a sum of a finite number of rank-one tensors, was first introduced by Hithcock in 1927 [21]. Later, Cattell proposed in 1944 the idea of parallel proportional analysis [22]. Afterwards, the concept gained popularity in 1970 in the form of CANDECOMP (canonical decomposition) by Carroll et al. [23]. Their work consisted of analyzing multiple variable data sets from a wide variety of subjects. The purpose was simply to do an average of the samples with respect to several points of view. On the other hand, Harshman [24] introduced PARAFAC, which allows to eliminate the ambiguity of the two-dimensional PCA

and has better uniqueness properties. Nowadays, it is commonly referred as CP decomposition (CANDECOMP/PARAFAC) introduced by Kiers [25].

In reality, CP Decomposition is a special case of the *Tucker Decomposition* when the so-called *core tensor* is superdiagonal (see Section 3.7).

Ordinary SVD leads to a very simplified solution, which translates into a fast recognition of the most relevant modes of the two-dimensional data set. On the other hand, HOSVD consists on decomposing an N^{th} order tensor into a *core tensor* and N side matrices, being N the order of the original tensor. On the contrary of the SVD, the core tensor is not usually diagonal, so it is desirable to simplify it in order to have an easy interpretation of the most significant modes of the system. The first approach to simplify the core tensor was developed by Kroonenberg & De Leeuw in 1980 [26] using the Alternating Least Squares (ALS) algorithm. Briefly explained for a case of a third order tensor, this algorithm starts with three initial orthonormal matrices \mathbf{G} , \mathbf{H} and \mathbf{E} . Two of them are fixed while the third one is optimized (in terms of minimum error) by means of an eigenvector problem. After convergence of the three matrices, the core tensor is simplified. A second approach can be done by estimating orthonormal transformations of the core tensor until reaching a simplified array [27]. These two approaches can be very time-consuming and they are not suitable for tensors of order higher than three. Besides, core tensors cannot be simplified to be completely diagonal so there is still a problem related with the interpretation of core arrays. The third approach was introduced by Henrion et al. [28] in 1999. This approach is based on the variance-of-squares measure and the fact that the squared core entries reflect the significance of the mode combinations in the system. Then, this method allows to extract the most relevant mode combinations from comparing the square of each entry with the sum of the squared entries of the whole core tensor. Besides, this approach does not need any prior assumption on the structure so it can be applied to any core tensor without regarding its shape. This final approach has resulted to be the most efficient for the extraction of the results for this thesis. There are other simplifications of the core tensor in the literature but they are referred to particular cases. For instance, Murakami et al. [29] performed a simplification of a core tensor of size $P \times Q \times R$ when $P = QR - 1$. In addition, Kiers & Berge [30] developed an extreme simplification for $3 \times 3 \times 3$ core tensors.

Finally, multilinear modal decomposition has been used in a wide variety of fields which involve large amount of multivariable data. A few examples are the application in image processing and denoising [31], in a fluorometric study [27] and in the classification of algae species through a fluorescence spectroscopic study [28].

3 Mathematical background

In this section, all the mathematical methodology of the decompositions mentioned in the previous section is briefly explained.

First, there is a small remark to understand the notation follow in this thesis. Then, all the matrix decomposition methods are explained. Afterwards, some preliminary concepts of tensor calculus are introduced to fully understand the later decomposition methods for tensors. Lastly, the Matlab matrix notation is explained in order to ease the reading of the project.

This section is mainly inspired by the works of Taira et al. [32], Lathauwer et al. [19] and Kolda & Bader [33].

3.1 Notation

Hereafter, in order to avoid confusion, the notation will follow some rules. Scalars will be denoted as lower-case letters (a, b, c, \dots), vectors as lower-case letters with an arrow above ($\vec{a}, \vec{b}, \vec{c}, \dots$) or also by bold lower-case letters ($\mathbf{a}, \mathbf{b}, \mathbf{c}, \dots$); matrices are represented by bold capital letters ($\mathbf{A}, \mathbf{B}, \mathbf{C}, \dots$) and tensors as calligraphic letters ($\mathcal{A}, \mathcal{B}, \mathcal{C}, \dots$). The coordinates of a tensor are depicted as (i, j, k) , e.g., the element at 1st row, 3rd column and 2nd tube of tensor \mathcal{A} is \mathcal{A}_{132} . The index of an element at the end of a given dimension is depicted as the capital letter of that dimension, e.g., $i = 1, 2, \dots, I$.

3.2 Eigenvalue Decomposition

This type of decomposition can be only applied to square matrices when the rank coincides with the domain of the matrix. So that, this procedure is very limited.

First of all, let introduce the concept of *eigenvalue* and *eigenvector*. An eigenvector (\vec{v}) and an eigenvalue (λ) are defined in such a way that the following expression is satisfied.

$$\mathbf{A}\vec{v} = \lambda\vec{v} \tag{1}$$

Where $\mathbf{A} \in R^{n \times n}$, $\vec{v} \in R^n$ and λ is a scalar. The eigenvalue decomposition starts with:

$$\mathbf{A}\mathbf{V} = \mathbf{V}\mathbf{\Lambda} \quad (2)$$

Such that \mathbf{V} is the matrix form by the eigenvectors of \mathbf{A} as column vectors and $\mathbf{\Lambda}$ is a diagonal matrix composed by the eigenvalues of \mathbf{A} .

$$\mathbf{V} = [\vec{v}_1, \vec{v}_2, \dots, \vec{v}_n]$$

$$\mathbf{\Lambda} = \text{diag}(\lambda_1, \lambda_2, \dots, \lambda_n)$$

Finally the eigenvalue decomposition results in:

$$\mathbf{A} = \mathbf{V}\mathbf{\Lambda}\mathbf{V}^{-1} \quad (3)$$

3.3 Singular Value Decomposition (SVD)

The SVD can be applied to any matrix independtly of its shape and rank so it is less limited than the eigenvalue decomposition.

SVD starts assuming that:

$$\mathbf{A}\vec{v}_j = \sigma_j \vec{u}_j \quad (4)$$

In matrix form:

$$\mathbf{A}\mathbf{V} = \mathbf{\Sigma}\mathbf{U} \quad (5)$$

Where $\mathbf{A} \in R^{m \times n}$, $\mathbf{V} \in R^{n \times n}$, $\mathbf{U} \in R^{m \times m}$ and $\mathbf{\Sigma}$ is a diagonal matrix composed by the singular values of matrix \mathbf{A} ($\sigma_1 \geq \sigma_2 \geq \dots \geq \sigma_n$)

The Singular Value Decomposition results in:

$$\mathbf{A} = \mathbf{U}\mathbf{\Sigma}\mathbf{V}^T \quad (6)$$

In order to obtain the SVD of a matrix \mathbf{A} , the matrices \mathbf{U} and \mathbf{V} are composed by the eigenvector of the matrix $\mathbf{A}\mathbf{A}^T$ and $\mathbf{A}^T\mathbf{A}$ respectively. On the other hand, the singular values (σ_j) are the square root of the eigenvalues of either matrices $\mathbf{A}\mathbf{A}^T$ or $\mathbf{A}^T\mathbf{A}$.

SVD is typically used for dimensionality reduction by reducing the rank of $\mathbf{\Sigma}$ eliminating the smallest singular values of the matrix.

3.4 Proper Orthogonal Decomposition (POD)

Proper Orthogonal Decomposition is a modal decomposition technique that identifies the modes of a flow field, e.g., in order to extract coherent structures from turbulent flows.

POD starts with an input vector field (e.g velocity) $\vec{q}(\xi, t)$ and assuming that it can be decomposed as follows:

$$\vec{q}(\xi, t) = \sum a_j \vec{\phi}_j(\xi, t) \quad (7)$$

Where $\vec{\phi}_j(\xi, t)$ represents the modes, a_j the expansion coefficients and ξ denotes the spatial component.

In order to have a better comprehension, it is helpful to split the space and time magnitudes, where $\vec{\phi}_j(\xi)$ denotes the spatial modes

$$\vec{q}(\xi, t) = \sum a_j(t) \vec{\phi}_j(\xi) \quad (8)$$

3.4.1 Classical POD Method

Starting from the input vector field $\vec{q}(\xi, t)$, the vector $\vec{x}(t)$ is the fluctuating term of the data vector with the time-averaged value $\bar{q}(\xi)$ removed such that:

$$\vec{x}(t) = \vec{q}(\xi, t) - \bar{q}(\xi) \quad (9)$$

Where $\vec{x}(t)$ is considered as a snapshot of the flow at time $t = t_1, t_2, \dots, t_n$.

The aim of POD is to find a set of vectors $\vec{\phi}_j(\xi)$ that best represents the flow data $\vec{q}(\xi)$ in an optimal way and with the least number of modes. In order to do that, the eigenvalue problem will be used for the next expression:

$$\mathbf{R} \vec{\phi}_j = \lambda_j \vec{\phi}_j \quad (10)$$

Where $\vec{\phi}_j \in R^n$, $\mathbf{R} = \mathbf{X} \mathbf{X}^T \in R^{n \times n}$ and $\mathbf{X} = [\vec{x}(t_1), \vec{x}(t_2), \dots, \vec{x}(t_m)] \in R^{n \times m}$.

The eigenvectors found from Eq. 10 are called *POD modes*.

If the eigenvalues of $\mathbf{X} \mathbf{X}^T$ are arranged from the largest to the smallest, it is possible to extract the more energetic modes of the flow field to be used in a future interpretation. With the most energetic modes, it is possible to show the most important behaviors of the flow by imposing Eq. 8, where the term a_j is the vectorial product of $\vec{x}(t)$ and $\vec{\phi}_j(\xi)$.

3.4.2 Method of Snapshots

When the sample n becomes very large, also does the eigenvalue problem since $\mathbf{R} = \mathbf{X}\mathbf{X}^T \in R^{n \times n}$. The method of snapshots consist of solving a reduced eigenvalue problem to find the POD modes. This method takes a collection of snapshots $\vec{x}(t_i)$ $t_i = t_1, t_2, \dots, t_m$ ($m \ll n$) such that the important fluctuations in the flow field are well resolved in time:

$$\mathbf{X}^T \mathbf{X} \vec{\psi}_j = \lambda_j \vec{\psi}_j \quad (11)$$

Where $\vec{\psi}_j \in R^m$ and $\mathbf{X}^T \mathbf{X} \in R^{m \times m}$ instead of $R^{n \times n}$. Relating the eigenvalues, they are the same that in the previous procedure.

With the eigenvectors $\vec{\psi}_j$, the POD modes can be obtained according to the next equation:

$$\vec{\phi}_j = \mathbf{X} \vec{\psi}_j \frac{1}{\sqrt{\lambda_j}} \quad (12)$$

3.4.3 SVD and POD

The POD can be related to the SVD as follows:

$$\mathbf{X} = \mathbf{\Phi} \mathbf{\Sigma} \mathbf{\Psi}^T \quad (13)$$

This means that SVD can be applied to a matrix \mathbf{X} to obtain the POD modes $\vec{\phi}_j(\xi)$ (column vectors of matrix $\mathbf{\Phi}$). Furthermore, eliminating the smallest terms of the matrix $\mathbf{\Sigma}$ it is possible to obtain the most relevant modes of the flow field.

Fig. 1 illustrates the first and second modes, blue and red respectively, of an arbitrary snapshot matrix \mathbf{A} . Identifying the dimension n as the time domain and d as the spatial one, the time modes are the columns of matrix \mathbf{U} and the spatial modes are the rows of matrix \mathbf{V}^T .

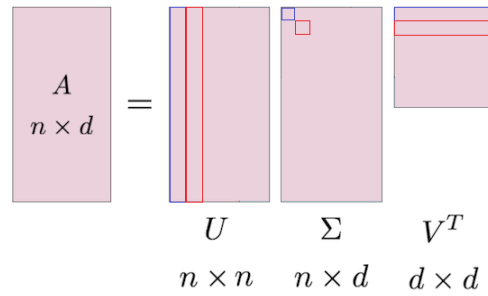


Figure 1: Illustration of the first mode (blue) and second mode (red). Adopted from [34].

3.5 Preliminary concepts of tensor calculus

3.5.1 Subtensors and fibers of a tensor

A *subtensor*, also known as a *slice*, is the result of fixing one dimension of the tensor, e.g., horizontal slices are obtained by fixing the i dimension and is depicted by $\mathcal{A}_{i::}$. A particular case is the frontal faces $\mathcal{A}_{::k}$ that can be simplified to \mathcal{A}_k .

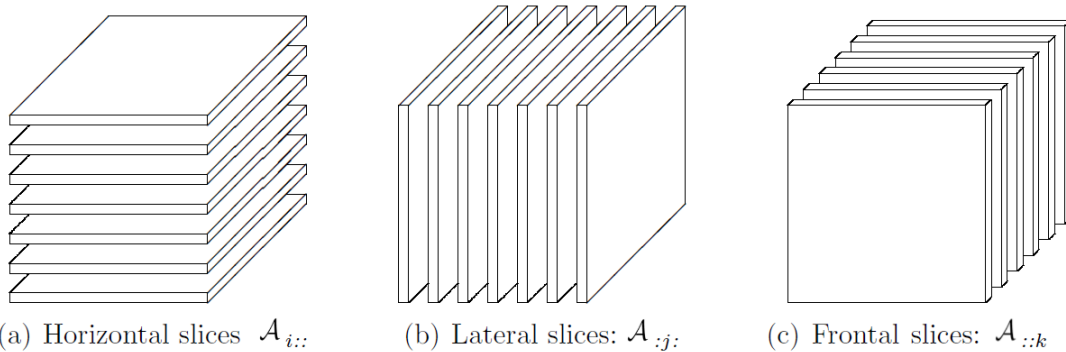


Figure 2: Subtensors of a 3^{rd} order tensor. Adopted from [33].

On the other hand, *fibers* are obtained by fixing two dimensions of the tensor, e.g., tube fibers (mode-3) are denoted as \mathcal{A}_{ij} .

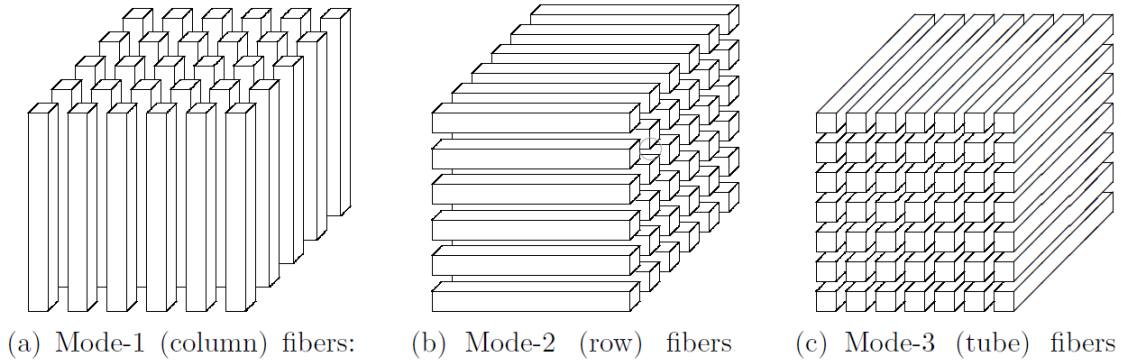


Figure 3: Fibers of a 3^{rd} order tensor. Adopted from [33].

Moreover, the Frobenius norm of a tensor $\mathcal{A} \in R^{I_1 \times I_2 \times I_3 \times \dots \times I_N}$ is the square root of the sum of the square of all its elements:

$$\|\mathcal{A}\| = \sqrt{\sum_{i_1=1}^{I_1} \sum_{i_2=1}^{I_2} \dots \sum_{i_N=1}^{I_N} x_{i_1 i_2 \dots i_N}^2} \quad (14)$$

3.5.2 Matricization

Matricization, also known as *unfolding*, is the process of arranging the terms of a tensor transforming a tensor into a matrix. Thus, an N^{th} order tensor can be unfolded in N different ways. For example, a $3 \times 5 \times 4$ tensor (3^{rd} order tensor) can be transformed as a 3×20 matrix, 5×12 and 4×15 matrix.

There are more than one method to perform the matricization but only the n -mode matricization will be explained since it is the most relevant for the case of study of this paper. The n -mode unfolding of a tensor \mathcal{A} is depicted as the matrix $\mathbf{A}_{(n)}$. The methodology is condensed in the next Figure.

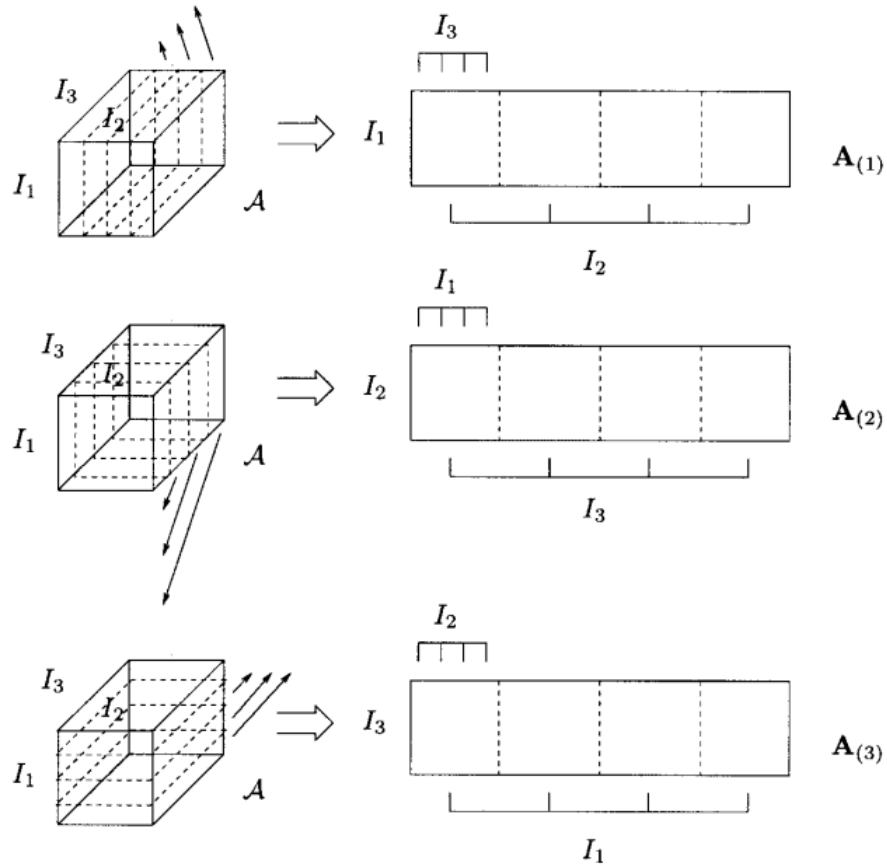


Figure 4: Matricization of a $I_1 \times I_2 \times I_3$ tensor. Adopted from [19].

The matrix $\mathbf{A}_{(1)}$ will have a shape of $I_1 \times I_2I_3$. In the same way, the dimensions of matrix $\mathbf{A}_{(2)}$ will be $I_2 \times I_3I_1$ and the matrix $\mathbf{A}_{(3)}$ will be a $I_3 \times I_1I_2$ matrix.

The best method to understand this procedure is with the use of an example.

Let the frontal slices of a tensor $\mathcal{A} \in \mathbb{R}^{3 \times 4 \times 2}$:

$$\mathbf{A}_1 = \begin{bmatrix} 1 & 2 & 3 & 4 \\ 5 & 6 & 7 & 8 \\ 9 & 10 & 11 & 12 \end{bmatrix}_{3 \times 4} \quad \mathbf{A}_2 = \begin{bmatrix} 13 & 14 & 15 & 16 \\ 17 & 18 & 19 & 20 \\ 21 & 22 & 23 & 24 \end{bmatrix}_{3 \times 4}$$

Then, the unfolded matrices of \mathcal{A} are:

$$\mathbf{A}_{(1)} = \begin{bmatrix} 1 & 2 & 3 & 4 & 13 & 14 & 15 & 16 \\ 5 & 6 & 7 & 8 & 17 & 18 & 19 & 20 \\ 9 & 10 & 11 & 12 & 21 & 22 & 23 & 24 \end{bmatrix}_{3 \times 8}$$

$$\mathbf{A}_{(2)} = \begin{bmatrix} 1 & 5 & 9 & 13 & 17 & 21 \\ 2 & 6 & 10 & 14 & 18 & 22 \\ 3 & 7 & 11 & 15 & 19 & 23 \\ 4 & 8 & 12 & 16 & 20 & 24 \end{bmatrix}_{4 \times 6}$$

$$\mathbf{A}_{(3)} = \begin{bmatrix} 1 & 5 & 9 & 2 & \dots & 4 & 8 & 12 \\ 13 & 17 & 21 & 14 & \dots & 16 & 20 & 24 \end{bmatrix}_{2 \times 12}$$

3.5.3 Matrix Kronecker product

The *Kronecker product* of two matrices $\mathbf{A} \in R^{I \times J}$ and $\mathbf{B} \in R^{K \times L}$ is denoted by $\mathbf{A} \otimes \mathbf{B}$. The result of this product is a $(IK) \times (JL)$ matrix defined by:

$$\mathbf{A} \otimes \mathbf{B} = \begin{bmatrix} a_{11}\mathbf{B} & a_{12}\mathbf{B} & a_{13}\mathbf{B} & \dots & a_{1J}\mathbf{B} \\ a_{21}\mathbf{B} & a_{22}\mathbf{B} & a_{23}\mathbf{B} & \dots & a_{2J}\mathbf{B} \\ \vdots & \vdots & \vdots & \ddots & \vdots \\ a_{I1}\mathbf{B} & a_{I2}\mathbf{B} & a_{I3}\mathbf{B} & \dots & a_{IJ}\mathbf{B} \end{bmatrix}$$

In order to better understand the *Kronecker product* let introduce, as an example, the matrices \mathbf{A} and \mathbf{B} and then compute the Kronecker product between them:

$$\mathbf{A} = \begin{bmatrix} 1 & 2 \\ 3 & 4 \end{bmatrix}; \mathbf{B} = \begin{bmatrix} 5 & 6 \\ 7 & 8 \end{bmatrix}$$

$$\mathbf{A} \otimes \mathbf{B} = \begin{bmatrix} 5 & 6 & 10 & 12 \\ 7 & 8 & 14 & 16 \\ 15 & 18 & 20 & 24 \\ 21 & 24 & 28 & 32 \end{bmatrix}$$

3.5.4 Khatri-Rao product

The *Khatri-Rao product* is defined as the "matching columnwise" Kronecker product. The Khatri-Rao product of matrices \mathbf{A} and \mathbf{B} is denoted by $\mathbf{A} \odot \mathbf{B}$. The result is a $(IJ) \times K$ matrix such that:

$$\mathbf{A} \odot \mathbf{B} = [a_1 \otimes b_1 \ a_2 \otimes b_2 \ \dots \ a_K \otimes b_L] \quad (15)$$

$$\mathbf{A} \odot \mathbf{B} = \begin{bmatrix} 5 & 12 \\ 7 & 16 \\ 15 & 24 \\ 21 & 32 \end{bmatrix}$$

3.5.5 Multiplication of a tensor by a matrix: n -mode product

The n -mode product is used to multiply a tensor times a matrix. The n -mode product of a tensor \mathcal{A} and a matrix \mathbf{U} is depicted as $\mathcal{A} \times_n \mathbf{U}$. The idea of this product is that the matrix \mathbf{U} multiplies every n -mode fibers of the tensor \mathcal{A} . This can also be seen in terms of matrix subtensors.

$$\mathcal{Y} = \mathcal{A} \times_n \mathbf{U} \Leftrightarrow \mathbf{Y}_{(n)} = \mathbf{U} \mathbf{X}_{(n)}$$

In order to match dimensions for the matrix product, the number of columns of matrix \mathbf{U} must coincide with the length of the n -mode fibers.

Again, the best method to understand this product is with an example. Let consider the tensor $\mathcal{A} \in R^{3 \times 4 \times 2}$ of section 3.5.2 and the matrix $\mathbf{U} \in R^{2 \times 3}$.

$$\mathbf{U} = \begin{bmatrix} 1 & 2 & 3 \\ 4 & 5 & 6 \end{bmatrix};$$

Then, the tensor \mathcal{X} is obtained as follows: $\mathcal{X} = \mathcal{A} \times_1 \mathbf{U}$.

$$\mathbf{X}_1 = \begin{bmatrix} 38 & 44 & 50 & 56 \\ 83 & 98 & 113 & 128 \end{bmatrix}; \mathbf{X}_2 = \begin{bmatrix} 110 & 116 & 122 & 128 \\ 263 & 278 & 293 & 308 \end{bmatrix};$$

3.6 Multilinear Singular Value Decomposition (MLSVD)

The MLSVD, also called *Tucker Decomposition* or *High Order Singular Value Decomposition* (HOSVD) consists on the decomposition of an N^{th} order tensor. The MLSVD for a 3^{rd} order tensor \mathcal{A} is illustrated in the next Figure.

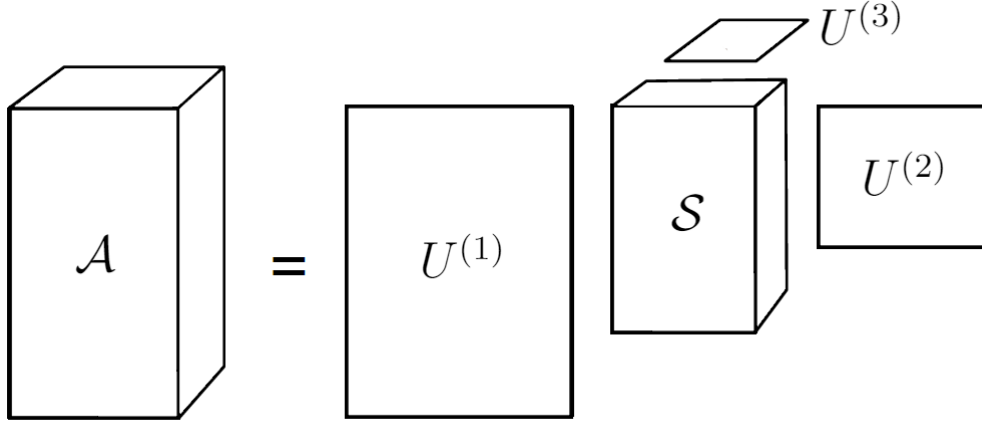


Figure 5: Visualization of a Tucker decomposition of a 3D tensor \mathcal{A} . Adopted from [33].

Since the MLSVD is used as a tool in this thesis, there is no need of a full explanation of the MLSVD algorithm. However, in case of more interest, the algorithm is well explained by Kiers & Kinderen [35].

The tensor $\mathcal{A} \in R^{I \times J \times K}$ is called *original tensor* and it is decomposed into a *core tensor* $\mathcal{S} \in R^{P \times Q \times R}$ and three matrices [$U^{(1)} \in R^{I \times P}$; $U^{(2)} \in R^{J \times Q}$; $U^{(3)} \in R^{K \times R}$].

Algebraically, the *MLSVD* of a complex $(I_1 \times I_2 \times \dots \times I_N)$ tensor \mathcal{A} can be written as the next product:

$$\mathcal{A} = \mathcal{S} \times_1 U^{(1)} \times_2 U^{(2)} \dots \times_n U^{(n)} \quad (16)$$

The matrix $U^{(n)}$ is quite similar with the side matrices in *SVD* in the sense that it is composed by orthonormal columns. The *core tensor* \mathcal{S} is composed by subtensors that fulfill the *all-orthogonality* property:

$$\langle \mathcal{S}_{in=\alpha}, \mathcal{S}_{in=\beta} \rangle = 0 \quad (17)$$

Eq. 17 means that every horizontal subtensors (i_1 is fixed) are mutually orthogonal. The same happens with the frontal (i_2 fixed) and vertical subtensors (i_3 fixed).

Each subtensor is ordered in descendent order as function of the Frobenius norm of each slice:

$$\|\mathcal{S}_{i_n=1}\| \geq \|\mathcal{S}_{i_n=2}\| \geq \dots \geq \|\mathcal{S}_{i_n=I_n}\| \geq 0 \quad (18)$$

This order is quite similar with the order of the singular values of the diagonal matrix of the SVD.

The entries of the *core tensor* \mathcal{S} measures the level of importance between the different elements. On the contrary of the diagonal matrix of the SVD, the entries of \mathcal{S} are not necessarily positive and real. Another important difference with the diagonal matrix of SVD is that the *core tensor* is not a purely diagonal tensor, which means that the only non-zero terms would be at indices $i_1 = i_2 = \dots = i_N$. Instead, \mathcal{S} fulfills the *all-orthogonality* property.

On the other hand, although the right matrix in SVD is transposed, $U^{(2)}$ has not been transposed because of symmetry reasons. Moreover, similarly than in the ordinary SVD, in MLSVD the modes are identified as the column vectors of each $U^{(n)}$ matrix, e.g., the modes of the J -dimension are represented in the columns of matrix $U^{(2)}$.

3.6.1 The n -rank

As in the SVD case, it is desirable to reduce the rank of the *core tensor* in order to better identify the most significant modes.

The rank of a tensor \mathcal{A} is denoted as $\text{rank}(\mathcal{A})$ and it is defined as the smallest number of rank-one tensors that generate \mathcal{A} . The definition of tensor rank is an exact analogue of matrix rank. However, the properties are not the same and the main difference is that there is no simply algorithm to obtain the rank of a tensor, e.g., the rank of a $9 \times 9 \times 9$ tensor can oscillate between 18 and 23.

Despite of this, in order to simplify the *core tensor*, it is needed to introduce the n -rank. Let \mathcal{A} an N^{th} order tensor of size $I_1 \times I_2 \times \dots \times I_N$. The n -rank of \mathcal{A} , denoted as $\text{rank}_n(\mathcal{A})$, is the column rank of matrix $A_{(n)}$. To have a better comprehension, let define $R_n = \text{rank}_n(\mathcal{A})$ for $n = 1, 2, \dots, N$. Then, it can be said that \mathcal{A} is a rank- (R_1, R_2, \dots, R_N) tensor. It is clear that $R_n < I_N$. Thus, the difference between tensor

rank and the n -rank is that for the latter it is used the matrix *unfoldings*. Note that both definitions are completely different.

The MLSVD saw in section 3.6 was a decomposition of \mathcal{A} where $R_n = \text{rank}_n(\mathcal{A})$. In order to reduce the size of the *core tensor* it is required to set the condition $R_n < \text{rank}_n(\mathcal{A})$ for one or more n . This method is known as *Truncated MLSVD* which is illustrated in the next Figure.

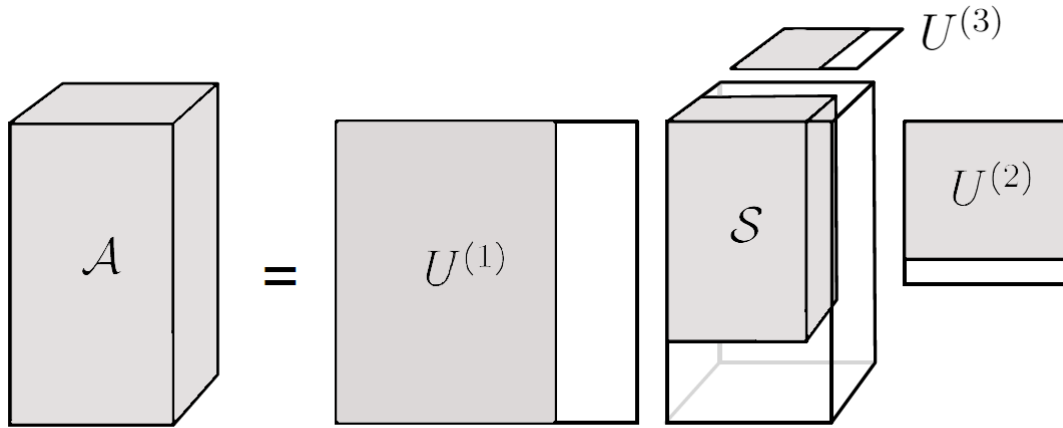


Figure 6: Truncated Tucker Decomposition. Adopted from [33].

One method to perform the *Truncated HOSVD* is using some equivalent representation of the Tucker Decomposition to try to see some relation between the matrix SVD and HOSVD. Taking advantage of the matrix *unfoldings*, the decomposition of tensor \mathcal{A} can be expressed as:

$$\mathbf{A}_{(n)} = \mathbf{U}^{(n)} \cdot \mathbf{S}_{(n)} \cdot (\mathbf{U}^{(n+1)} \otimes \mathbf{U}^{(n+2)} \otimes \dots \otimes \mathbf{U}^{(N)} \otimes \mathbf{U}^{(1)} \otimes \mathbf{U}^{(2)} \dots \otimes \mathbf{U}^{(n-1)})^T \quad (19)$$

An example for a third-order tensor would be:

$$\begin{aligned} \mathbf{A}_{(1)} &= \mathbf{U}^{(1)} \cdot \mathbf{S}_{(1)} \cdot (\mathbf{U}^{(3)} \otimes \mathbf{U}^{(2)})^T \\ \mathbf{A}_{(2)} &= \mathbf{U}^{(2)} \cdot \mathbf{S}_{(2)} \cdot (\mathbf{U}^{(3)} \otimes \mathbf{U}^{(1)})^T \\ \mathbf{A}_{(3)} &= \mathbf{U}^{(3)} \cdot \mathbf{S}_{(3)} \cdot (\mathbf{U}^{(2)} \otimes \mathbf{U}^{(1)})^T \end{aligned}$$

Now, let define a diagonal matrix $\Sigma^{(n)} \in R^{I_n \times I_n}$ and an orthonormal matrix $\mathbf{V}^{(n)} \in R^{I_{n+1}I_{n+2}\dots I_N I_1 I_2 \dots I_{n-1} \times I_n}$ such that:

$$\Sigma^{(n)} = \text{diag} \left(\sigma_1^{(n)}, \sigma_2^{(n)}, \dots, \sigma_{I_n}^{(n)} \right) \quad (20)$$

$$\mathbf{V}^{(n)H} = \tilde{\mathbf{S}}_{(n)} \cdot (\mathbf{U}^{(n+1)} \otimes \mathbf{U}^{(n+2)} \otimes \dots \otimes \mathbf{U}^{(N)} \otimes \mathbf{U}^{(1)} \otimes \mathbf{U}^{(2)} \dots \otimes \mathbf{U}^{(n-1)}) \quad (21)$$

In which $\sigma_i^{(n)}$ is the Frobenius norm of the rows of $\mathbf{S}_{(n)}$ and $\tilde{\mathbf{S}}_{(n)}$ is the normalized matrix of $\mathbf{S}_{(n)}$ defined as:

$$\mathbf{S}_{(n)} = \Sigma^{(n)} \cdot \tilde{\mathbf{S}}_{(n)} \quad (22)$$

Expressing Eq. 19 in terms of $\mathbf{V}^{(n)H}$ and $\Sigma^{(n)}$, the HOSVD results in a SVD matrix form:

$$\mathbf{A}_{(n)} = \mathbf{U}^{(n)} \cdot \Sigma^{(n)} \cdot \mathbf{V}^{(n)T} \quad (23)$$

Now, the least important diagonal terms of $\Sigma^{(n)}$ could be removed in order to simplify the MLSVD method.

3.7 CP Decomposition

CP Decomposition is the special case of the HOSVD when the core tensor is super-diagonal, i.e., $\mathcal{S}_{ijk} = 0$ if any two indices are distinct.

CP Decomposition, illustrated in Fig. 7, consists of obtaining the tensor \mathcal{X} as the sum of rank-one tensors. Given a tensor \mathcal{X} of size $I \times J \times K$, it is desirable to have the decomposition:

$$\mathcal{X} = \sum_{r=1}^R \mathbf{a}_r \circ \mathbf{b}_r \circ \mathbf{c}_r \quad (24)$$

Such that $r = 1, \dots, R$, $a_r \in R^I$, $b_r \in R^J$, $c_r \in R^K$. The outer product of two vectors is defined as:

$$\mathbf{u} \circ \mathbf{v} = \mathbf{u}\mathbf{v}^T \quad (25)$$

Elementwise, Eq. 24 can be expressed as:

$$x_{ijk} \approx \sum_{r=1}^R a_{ir} b_{jr} c_{kr} \quad (26)$$

For $i = 1, \dots, I$, $j = 1, \dots, J$ and $k = 1, \dots, K$.

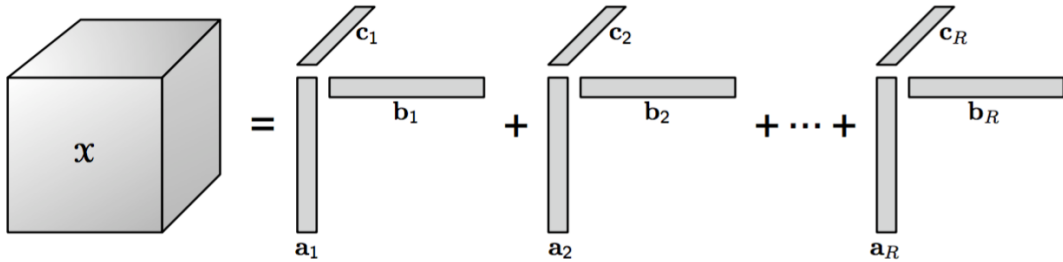


Figure 7: Illustration of the CP decomposition. Adopted from [33].

Although this particular case for which the CP Decomposition (core tensor is diagonal) cannot be applied in a general form, note that this rank-one tensors are similar to the columns of the matrix $\mathbf{U}^{(n)}$ of the HOSVD. In this way, the original tensor \mathcal{A} can be expressed as the outer product of the core tensor and these rank-one tensors:

$$\mathcal{A} = \sum_{i=1}^I \sum_{j=1}^J \sum_{k=1}^K \sum_{n=1}^N \mathcal{S}_{i,j,k,n} \circ \mathbf{U}_i^{(1)} \circ \mathbf{U}_j^{(2)} \circ \mathbf{U}_k^{(3)} \circ \mathbf{U}_N^{(n)} \quad (27)$$

A combination of the HOSVD and this multilinear modal decomposition form (Eq. 27) is the tensor decomposition method used during the development of this thesis.

3.8 Matlab matrix notation

In order to ease the reading of the next sections of the thesis, the Matlab matrix notation should be explained.

In fact, the Matlab notation for matrices is very similar to other programming languages such as Python or C/C++.

Let consider a 2-D matrix \mathbf{A} . Then the entry corresponding to the first row and second column will be denoted as $A(1,2)$. So, the first number means the row and the second number represents the column. In case of selecting just the second column of \mathbf{A} would be $A(:,2)$. Conversely, in case of selecting the third row would be $A(3,:)$. In contrary of other languages, the position index in Matlab starts at one instead of zero. In addition, in case of dealing with tensors, the third dimension would be denoted in the third position. For instance, to access to the second matrix with all the rows and columns would be $A(:, :, 2)$. The same procedure applies to an N^{th} order matrix.

4 Flapping wings parametric study

Flapping wings problems are very complex and they have not been well understood yet. Besides, they are influenced by a large number of parameters. In this way, it could be interesting to perform a multilinear decomposition over a flapping wing problem and make a parametric study of multiple variables at the same time.

This section introduces the problem of flapping wings through some kinematic concepts and a brief state of the art. Then, the motivation to apply a multilinear modal decomposition in this type of problems is discussed. Finally, the experimental procedure, from which the data is taken, is explained with some remarks in the data collection, the experimental sources of error and the tensor construction for its later modal decomposition.

4.1 Introduction of flapping wings

The main source of lift and propulsion in nature is flapping wings, which are present in fish, birds and insects. Nowadays, there is an increasing interest in the study of the aerodynamics of flapping wings due to its use in ornithopters [36], robotic fish [37] and micro air vehicles (MAVs). The operating conditions of MAVs are close to those in which birds and insects actually fly: a low Reynolds (Re) number, a high amplitude and moderate frequency motion [38]. For a better design of MAVs, a deep study of the aerodynamics of flapping wings is crucial.

First, let introduce some kinematic concepts of flapping wings. The motion of a flapping wing is governed by two harmonic oscillations: *pitching* and *plunging*, also called *heave*.

- **Pitch motion.** The pitching is the rotation about a wing pivot point and its expression is:

$$\theta(t) = \theta_m + \theta_0 \sin(2\pi ft + \phi) \quad (28)$$

In which θ_m is the mean pitching angle, θ_0 is the pitching amplitude, f is the motion oscillation frequency and ϕ is the phase lag angle between the pitch and plunge motion.

- **Plunge motion.** The plunging, also called heave, is the vertical wing displacement whose mathematical expression is:

$$h(t) = h_0 \sin(2\pi ft) \quad (29)$$

Where h_0 is the plunging amplitude.

These two motions are illustrated in Fig. 8 and 9.

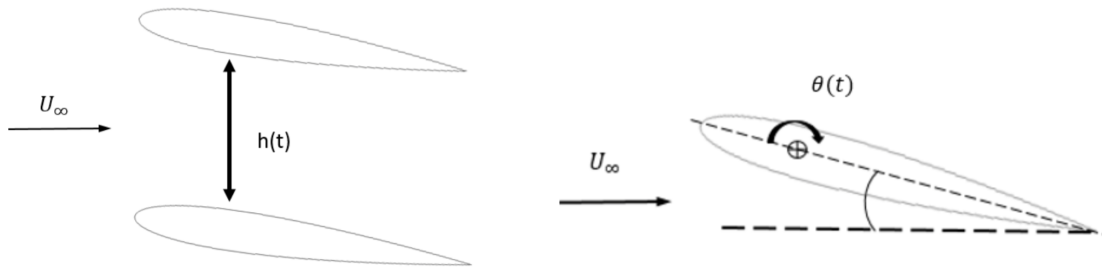


Figure 9: Pitch motion. Adopted from [2].

Figure 8: Plunge motion. Adopted from [2].

To make these two motions more clear, Fig. 10 shows the combination of these two motions: heave and a 180° pitching.

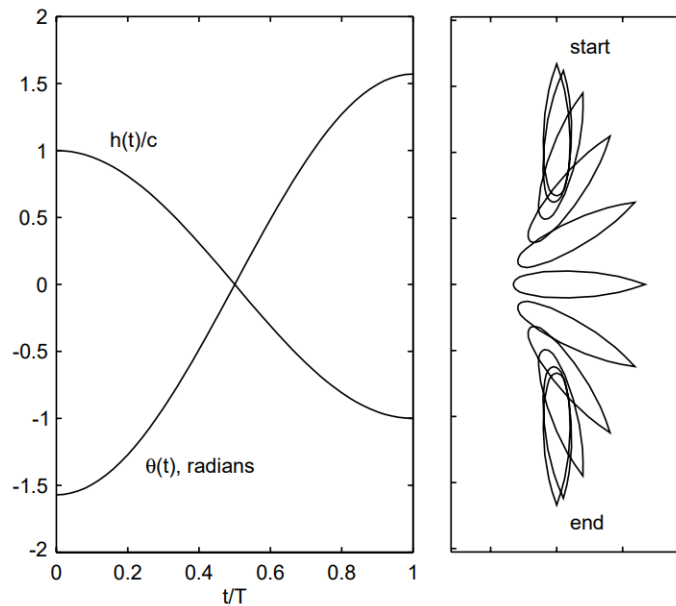


Figure 10: Airfoil trajectory combining heave motion and a 180° pitch change. Adopted from [39].

These two motions result in an effective angle of attack given by the following equation:

$$\alpha_{eff}(t) = \theta_m + \theta_0 \sin(2\pi ft + \phi) - \text{atan}\left(\frac{1}{U_\infty} \frac{dh}{dt}\right) \quad (30)$$

Another important parameter in flapping wings is the *Strouhal number* (St), which is defined as the dimensionless number given by the following expression:

$$St = \frac{2fh_0c}{U_\infty} \quad (31)$$

The first study of flapping wings was carried out by Leonardo Da Vinci in 1505 when he tried to make a man powered ornithopters [40].

Later, at the beginning of the twentieth century, independently Knoller (1909) [41] and Betz (1912) [42] noted that the vertical movement of an airfoil produces an effective angle of attack and an aerodynamic force that could be decomposed as lift, in the perpendicular direction of flight, and thrust, in the direction of flight. In 1922, Katzmayr [43] made the first experimental observations of this phenomena and Ober (1925) [44] gave some theoretical explanations to this topic.

In 1935, Theodorsen [45] carried out theoretical computations of an airfoil under small amplitude plunging leading to the conclusion that all pure plunging motions generate thrust, which is proportional to the square of the frequency of the motion. Moreover, another conclusion he obtained was that the propulsion efficiency approaches to 1.0 as the frequency of the heaving motion approaches to zero and that the efficiency behaves asymptotically with a value of 0.5 at high frequencies of heave motion. Additionally, in 1936, Garrick [46] used Theodorsen's work to obtained that the drag in a flapping wing can be split in two contributions: the pressure force acting along the airfoil and the leading-edge suction. Later, Theodorsen in 1949 [47] developed a complete theory based on potential flow that was able to predict the aerodynamic forces on a thin airfoil for small-amplitude motions at high Re .

Thanks to experiments, Freymuth [48] discovered in 1988 that the drag wake is analogous to the von Kármán street behind a bluff body. Also demonstrated that any airfoil under either pure pitching or pure plunging generates a thrust force.

It is acknowledged in the flapping wings field that the performance highly depends on the formation of leading edge and trailing edge vortices (LEV and TEV). Ellington et al. [49] discovered that the formation of a LEV is the main mechanism of lift

generation in flapping wings. Streitlien et al. [50] demonstrated experimentally the effect of the interactions between the LEV and TEV on the thrust and propulsive efficiency. In addition, Anderson et al. [51] stated that the optimum propulsion efficiency happens at an specific level of interaction between the leading edge and trailing edge vortices.

As in fixed-wing aerodynamics, an increase of the angle of attack will translate into an increase of lift but as long as the LEV remains attached to the foil. If the angle of attack continues increasing, there will be a point in which the flow separates at the leading edge followed by a sudden drop of lift force. This phenomenon is called *dynamic stall* [52]. It has been theorized that many insects fly at the limit of dynamic stall, where high lift coefficients are generated after a sudden change in the effective angle of attack [53] [54].

Furthermore, Read et al. [39] performed an experiment varying the heave and pitching phase angle obtaining the conclusion that a phase angle of 90 - 100° gives the best thrust performance.

4.2 Objective of the study

The aerodynamic forces acting on flapping wings have been tried to assess using complex models. An example is the one developed by Hall & Hall [55] who takes advantage of vortex lattice method to extract the optimal circulation distribution for a certain lift and thrust force. This vortex lattice method works without regarding the geometry or the airfoil movement. However, as it is based on potential flow theory, this model does not include flow separation. This method was improved by Hall, Pigott & Hall [56] including viscous drag effects. Jones, Dohring & Platzer [57] developed another model to determine the wake of a flapping airfoil under plunging and pitching which resulted to be very accurate with the experimental data, obtaining the conclusion that the wake evolution is mainly due to an inviscid phenomenon.

These models try to describe the complex physical phenomena under flapping motion but modal decomposition allows to perform a simpler parametric study. With a modal decomposition, it can be easily seen how each parameter affects individually to the system without the necessity of entering into too much detail in the fluid mechanics field.

N-way principal component analysis permits to performed a modal decomposition of more than two parameters at the same time. This thesis will be focused on the parametric study of the pitching amplitude (θ_0), the mean pitching angle (θ_m) and the *Strouhal number* (St) based on the experimental data set obtained by María del Mar Carrillo [2].

4.3 Experimental data set details

4.3.1 Data collection

The data set analyzed is an experimental data set taken by María del Mar Carrillo [2] carried out in the water tunnel facility of the Aerospace Engineering department of the Universidad Carlos III de Madrid. Using this data set, Carrillo studied the influence of certain parameters on the C_L and C_D of a flapping wing.

For all the experiments, the wing tested was a rectangular wing NACA0012 airfoil with a chord of 0.03m, a thickness-to-chord ratio $\frac{t}{c} = 0.12$, a span of 0.49 m and an aspect ratio of 16.3m. The experiment was done under low *Reynolds number* ($Re \approx 3500 - 3600$), $Re = \frac{U_\infty c}{\nu}$, with a plunging amplitude (h_0) equals to the wing chord under an upstream velocity (U_∞) equals to 0.12 m/s and assuming air as the working fluid with a dynamic viscosity of the order of $10^{-5} m^2/s$. The phase angle ϕ between heave and pitching has been set to 90° . The flapping frequencies are 0.2 *Hz*, 0.4 *Hz* and $f=0.6$ *Hz* which gives three values of St : $St = 0.1$, $St = 0.2$ and $St = 0.3$ respectively.

The experiments could have been done either in a water or a wind tunnel. However, the forces measured in a water tunnel are larger so the overall force resolution is also better. The difference in force magnitude of air and water is shown in Eq. 32.

$$\frac{F_{water}}{F_{air}} = \frac{\frac{1}{2}\rho_{water}U_{water}^2}{\frac{1}{2}\rho_{air}U_{air}^2} \approx 10 \quad (32)$$

On the other hand, the time parameter was made dimensionless by dividing the time by the period (t/T), taking values from 0 to 1. The values of mean pitch angle (θ_m) and the ones of pitch amplitudes (θ_0) chosen for the experiment goes from 0° to 15° with an interval of 5 degrees. The values of the different parameters in the experiment are summarized in Table 1.

θ_0	$0^\circ - 5^\circ - 10^\circ - 15^\circ$
θ_m	$0^\circ - 5^\circ - 10^\circ - 15^\circ$
t/T	0 - 1 (in 100 steps)
St	0.1 - 0.2 - 0.3

Table 1: Values of parameters

4.3.2 Sources of error

In the experiment carried out by Carrillo [2], there are three main sources of error:

- **Error due to sensor bias.** When the sensor is turned on, the strain gauges of it starts to emit power proportional to the product of the gauge resistance and the square of the current. This is called the *Joule's effect*. This bias error was already corrected by Carrillo in her work [2].
- **Sensitivity error or random error.** As it is a random, Carrillo [2] removed this error easily after a long measurement since it decreases with the square root of samples measured.
- At the time of performing the experiment, in order to join the sensor to the wing and to the rod mechanism, a L-type beam is used. This support mechanism implies that the centre of pitching is not in the wing, but 12 mm vertically displaced. This will produce an azimuthal component of the velocity during the pitching motion. For a general rotation, the azimuthal component of the velocity is given by the following equation:

$$V_h = r\dot{\theta} = 2\pi r f \theta_0 \cos(2\pi f t + \phi) \quad (33)$$

Where $r = 12mm$.

This velocity causes an unavoidable error. Nevertheless, the maximum value of this azimuthal velocity is $0.016 m/s$, so it will not be noteworthy for the results.

4.3.3 C_L and C_D rotation

At a first instance, the modal decomposition would be performed on C_L and C_D coefficients. However, the results obtained were not smooth enough. This is the reason why the modal analysis has been applied to the vertical and horizontal force coefficients instead, C_Y and C_X respectively.

$$C_Y = \frac{F_Y}{\frac{1}{2}\rho S U_\infty^2} \quad (34)$$

$$C_X = \frac{F_X}{\frac{1}{2}\rho S U_\infty^2} \quad (35)$$

In order to do the conversion from C_L and C_D to C_Y and C_X , a projection with respect to the angle θ has to be performed according to Fig. 11 and Eq. 36 and 37:

$$C_Y = C_L \cos \theta + C_D \sin \theta \quad (36)$$

$$C_X = -C_L \sin \theta + C_D \cos \theta \quad (37)$$

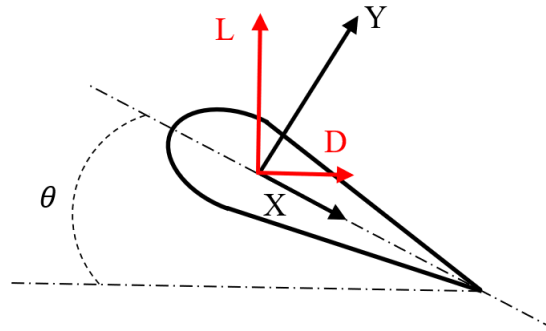


Figure 11: Scheme of the rotation of C_L and C_D .

4.3.4 Tensor construction

HOSVD was used to perform a parametric study to see the influence of θ_0 , θ_m and the Strouhal number (St) on C_X and C_Y over time.

As can be seen in Section 4.3.2, the error is mainly concentrated on the mean value of the force. For this reason, the mean value of each experimental data was removed at the time of constructing the tensor. In this way, the parametric study was focused only on the fluctuating part of the force coefficients.

The data set for C_Y and C_X was located in a fourth-order tensor \mathcal{C}_Y and $\mathcal{C}_X \in R^{4 \times 100 \times 4 \times 3}$ in which the first dimension ($i = 1, 2, 3, 4$) means the variation of θ_0 , the second ($j = 1, 2, \dots, 100$) identifies the dimensionless time variable, the third one ($k = 1, 2, 3, 4$) means the θ_m parameter and the fourth dimension ($l = 1, 2, 3$) means the St variation, i.e., $\mathcal{C}_Y \in R^{\theta_0 \times t \times \theta_m \times St}$. The coefficient letter corresponding to each parameter is summarized in Table 2.

Parameter	Coefficient
θ_0	i
t/T	j
θ_m	k
St	l

Table 2: Coefficient letter corresponding to each parameter.

After the simulation, the results are a *core tensor* \mathcal{S} of size $4 \times 20 \times 4 \times 3$, and the matrices $U^{(n)}$ are [$U^{(1)} \in R^{4 \times 4}$; $U^{(2)} \in R^{100 \times 20}$; $U^{(3)} \in R^{4 \times 4}$; $U^{(4)} \in R^{3 \times 3}$].

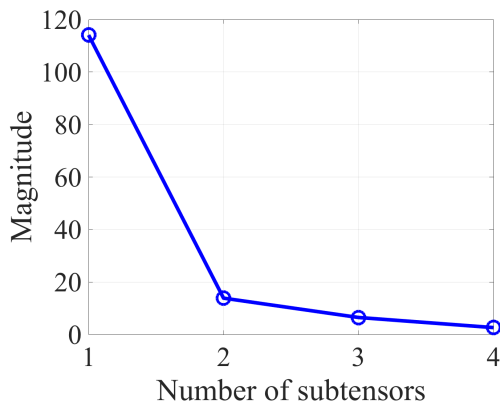
Consequently, as detailed in Section 3.6, the columns of the matrices $U^{(n)}$ are identified with the modes of the n parameter. In this particular flapping wing data set, the columns of $U^{(1)}$ identify the modes of the parameter θ_0 , $U^{(2)}$ with *dimensionless time*, as well as $U^{(3)}$ with θ_m and $U^{(4)}$ with St .

5 Results

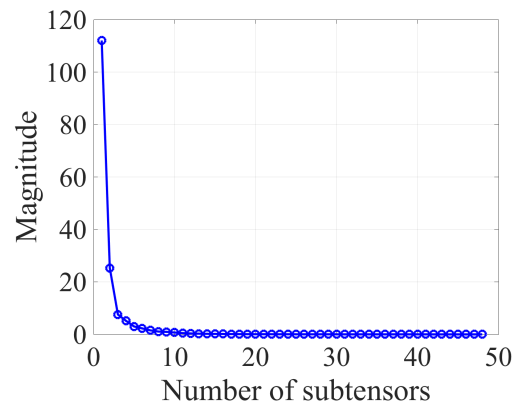
This section shows the results after performing the multilinear modal decomposition of the tensor of both force coefficients studied, C_Y and C_X respectively. In addition, the application of the called *comparison method* and the coefficient of determination are explained to have a better discussion of the results. The modes obtained are compared with the experimental results obtained by Carrillo [2] to proof the validity of the multilinear modal decomposition.

5.1 Parametric study of C_Y .

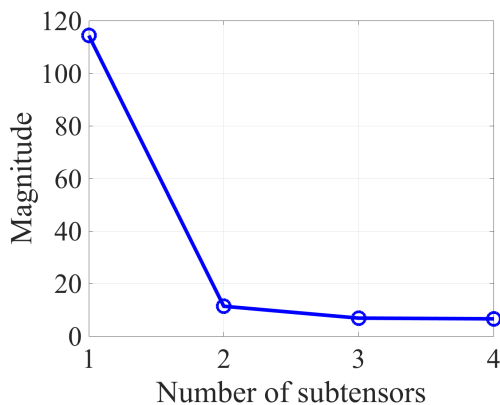
The Frobenius norm of the subtensors of the core tensor obtained by fixing one parameter are depicted in Figure 12a, 12b, 12c and 12d.



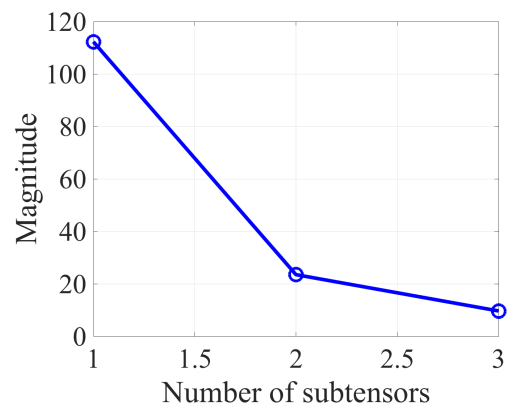
(a) Frobenius norm of θ_0 subtensors.



(b) Frobenius norm of time subtensors.



(c) Frobenius norm of θ_m subtensors .



(d) Frobenius norm of St subtensors.

Figure 12

Fig. 12a, 12c 12b and 12d show that the different subtensors of the tensor \mathcal{C}_y are ordered in a descendent way as already explained in Eq. 18. Now, let focus on Fig. 12b which has a large sample. It is clear that the most significant subtensors are the first three ones while the rest can be considered as noise and they are not relevant for the aim of the parametric study.

Regarding the parametric study, the output of the HOSVD is much more complicated to interpret than the case of the ordinary matrix SVD. The main issue is that the core tensor is not diagonal. However, as seen in Figure 12b, the entries of the core tensor are organized in descendent order, also seen in [19]. In other words, the most relevant entries of the core tensor are located at low values of i, j, k, l . This property was used by Henrion et al. [28] reducing the size of the core tensor in order to remove the least relevant entries of the tensor and to decrease computation time. In the case of the present paper, the core tensor is truncated up to a $3 \times 3 \times 3 \times 3$ tensor. Although this truncation may be seen severe, the reality is that the tensor still has 81 (3^4) rank-one tensors that have to be analyzed (instead of the 4,800 rank-one tensors of the original tensor) which means that no relevant information is missing after the truncation. To summarize, this truncation has the power of simplifying the original tensor as well as get rid of the non-relevant rank-one tensors, which translates into a large reduction in computation time. Of course, this truncation has an effect on the *all-orthogonality* property of the core tensor, but this property does not have any relevance at the time of performing a parametric study.

After this truncation, the comparison of the square of each core tensor entry is performed with respect to the sum of the squared entries of the whole tensor. The comparison is shown in Table 3. According to the rank-one tensor property explained in Section 3.7, the coefficients of each entry (i, j, k, l) are related to their corresponding modes in the following way: $\mathbf{U}_i^{(1)}$, $\mathbf{U}_j^{(2)}$, $\mathbf{U}_k^{(3)}$ and $\mathbf{U}_l^{(4)}$ as seen in Eq. 38.

$$\mathcal{A} = \sum_{i=1}^I \sum_{j=1}^J \sum_{k=1}^K \sum_{l=1}^L \mathcal{S}_{i,j,k,l} \circ \mathbf{U}_i^{(1)} \circ \mathbf{U}_j^{(2)} \circ \mathbf{U}_k^{(3)} \circ \mathbf{U}_l^{(4)} \quad (38)$$

Hereafter, this method will be called *comparison method*.

n	(i, j, k, l)	$\mathcal{S}_{i,j,k,l}^2 / \sum \mathcal{S}_{i,j,k,l}^2 (\%)$
1	(1,1,1,1)	93.82
2	(1,2,1,2)	3.50
3	(2,1,1,2)	0.43
4	(2,2,1,1)	0.37
5	(1,2,2,1)	0.35
6	(2,1,1,3)	0.28
7	(2,2,1,1)	0.19

Table 3: Leading mode combinations of C_Y according to the *comparison method*.

Table 3 shows the effect of the parameters for the overall set of cases. The values of the right column represent the relative weight of the particular mode combination to the whole system. As expected, the combination of the first mode of each parameter (1,1,1,1) is the most relevant one, since the core tensor and side matrices are organized in descendent order [19]. On the other hand, the combination of the first θ_0 mode, the second mode of the time, the first mode of θ_m and second mode of the St , (1,2,1,2), has a less impact on the system, but still plays an important role as it will be discussed later. The rest of the combinations seems to have a negligible effect on the average of C_Y over the entire ensemble.

After the development of the *comparison method*, it is needed to show its validity comparing the results obtained by the *comparison method* with the experimental data obtained by Carrillo [2].

Fig. 13 shows the effect of the variation of θ_0 (Fig. 13a), θ_m (Fig. 13b) and St (Fig. 13c) parameters on the C_Y over time. These figures will be very helpful at the time of discussing the results obtained with the MLSVD and the *comparison method*.

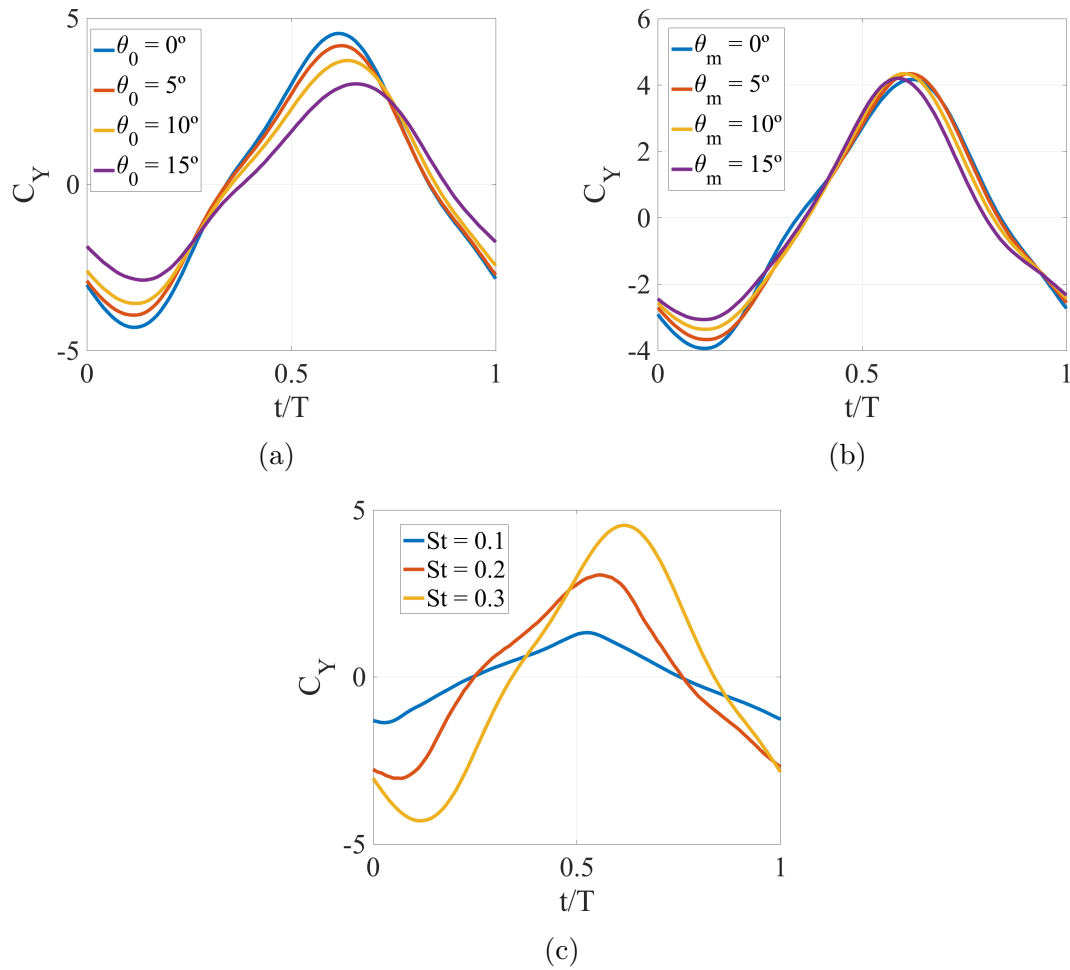
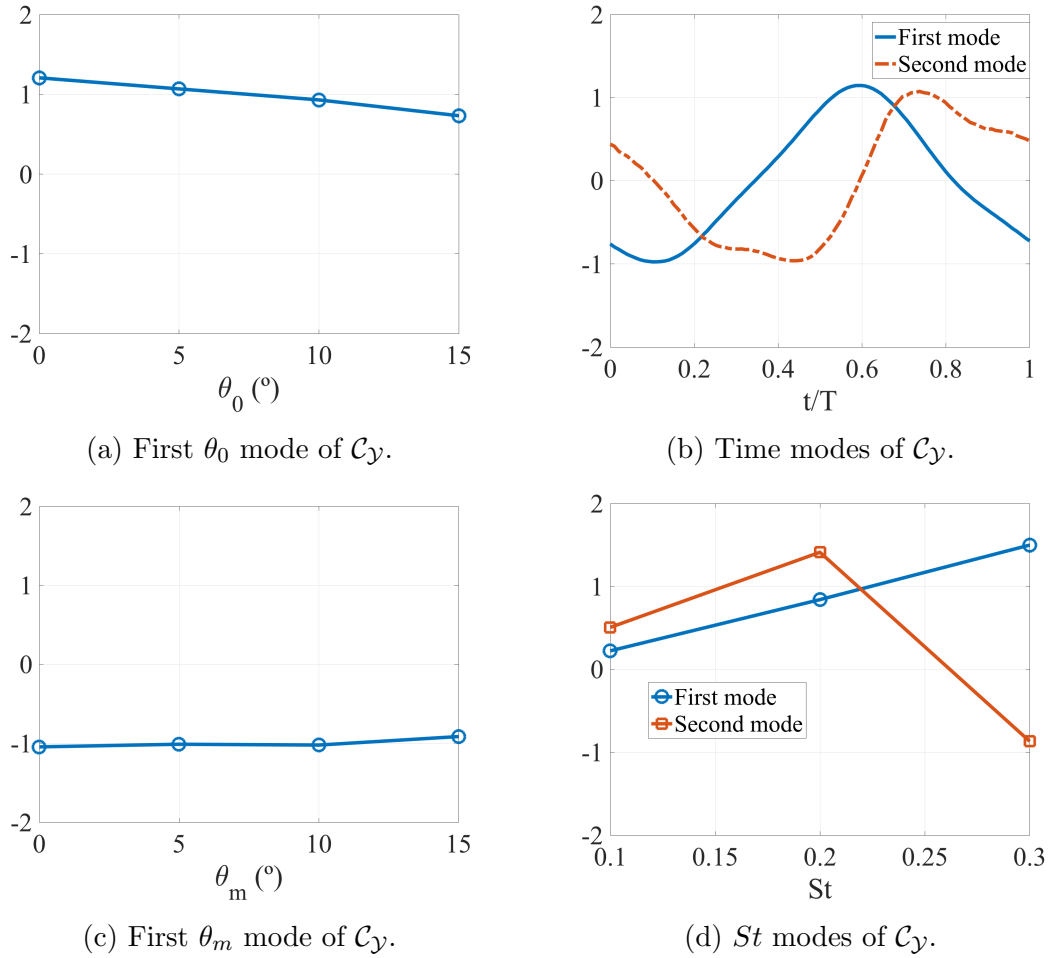


Figure 13: (a) θ_0 effect on C_Y with $\theta_m = 0^\circ$ and $St = 0.3$; (b) θ_m effect on C_Y with $\theta_0 = 5^\circ$ and $St = 0.3$; (c) St effect on C_Y with $\theta_0 = 0^\circ$ and $\theta_m = 0^\circ$.

Moreover, Fig. 14 shows the most relevant modes of the C_Y tensor according to the *comparison method* seen in Table 3.

First of all, the first time mode of Fig. 14b shows clear sinusoidal dependency of C_Y with time. Indeed, this shape is the one that appears in almost all the cases of C_Y as can be seen in Fig. 13b for instance.

Figure 14: Most relevant modes of C_Y .

Furthermore, the effect of the first θ_0 mode (Fig 14a) is very close to be linear, with a slope of -0.129 deg^{-1} , in such a way that if θ_0 increases, the amplitude of C_Y decreases as seen in Fig. 13a.

On the other hand, the behavior of the first θ_m mode is almost constant (with a little positive slope of 0.0043 deg^{-1}) which can be translated into a no relevant effect of θ_m on C_Y . Having the reference of Fig. 13b, it can be seen that there is no relevant tendency while changing the θ_m parameter.

The first *Strouhal* mode (Fig. 14d) behaves like a linear function with a slope of 6.3745. This linear tendency can be seen in Fig. 13c where an increase of the St means an increase of the amplitude of the force coefficient.

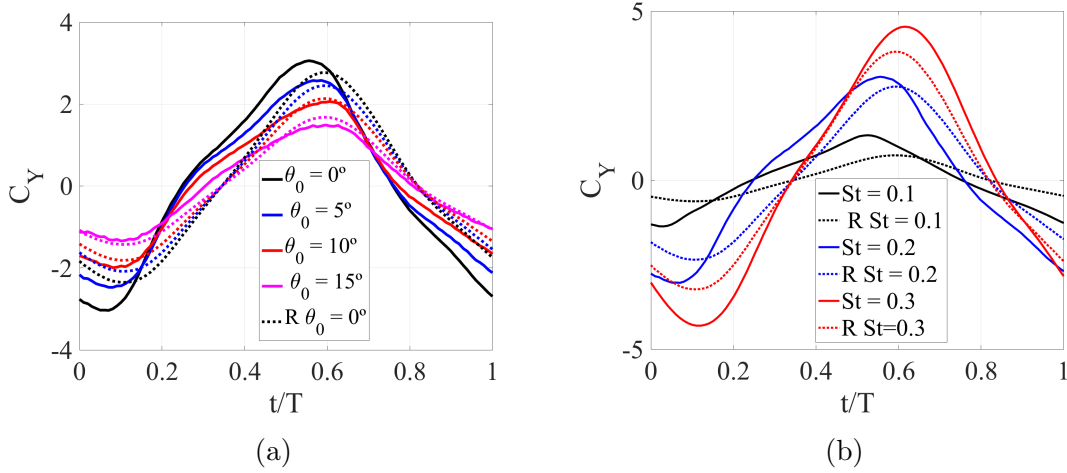


Figure 15: (a) C_Y variation with θ_0 ($\theta_m = 0^\circ$ and $St = 0.2$) and the reconstruction using just the most relevant mode combination; (b) C_Y variation with St ($\theta_0 = 0^\circ$ and $\theta_m = 0^\circ$). Reconstruction cases are depicted in dotted lines.

In addition, Fig. 15a and 15b show the curves obtained after performing the reconstruction with only the first mode combination (dotted lines). These two figures show, with more clarity, the effect of the first θ_0 mode (Fig. 15a), which is a decrease of the amplitude of C_Y as θ_0 increases, and the effect of the first mode of St (Fig. 15b), the increase of the amplitude of C_Y as *Strouhal number* increases.

The second relevant combination of modes (1, 2, 1, 2) is exactly the same for the modes of θ_0 and θ_m but the time and St modes change. The second time mode (Fig. 14b in red) has the shape of a nearly sine function (it is still a periodic function) but it is shifted to the right (around 90°) with respect to the first mode. The contribution of the two time modes (with a larger contribution of the first mode) leads to a shift to the right. This shift can be easily seen in Fig. 13c where it is very appreciable the effect of the first two time modes. In addition, the impact of this shift is even more clear in Fig. 15a and 15b where, as the second time mode has not been considered to perform the reconstruction, no shift appears in the reconstruction cases.

Moreover, in the second mode of the *Strouhal number* (Fig. 14d) can be seen what Triantafyllou et al. [58] discovered experimentally. They discovered that the point of maximum efficiency of lift generation lies between a range of *Strouhal number* of $0.25 \leq St \leq 0.35$. In addition, it has been assessed that swimming animals actually operates at the same range of *Strouhal* [59]. A data with more measured points would make to see this conclusion in a clearer way.

Although the *comparison method* was first introduced by Henrion et al. [28], they

did not show its validity with a much more confident tool than simply comparing the results with the experimental data. A much more reliable tool for analyzing the validity of the *comparison method* is the coefficient of determination (R^2). The coefficient of determination, introduced by Wright [60] and used by Devore [61] and Cameron [62] among others, can be used to determine how close the reconstruction, using just a few combination of modes, is compared to the real function. In the present paper, the function is the different time vectors of the tensor $\mathcal{C}_y(i, :, k, l)$ denoted in Table 4 following the Matlab notation.

$$R^2 = 1 - \frac{SS_{res}}{SS_{tot}} \quad (39)$$

Where:

$$SS_{res} = \sum (y - f)^2, \quad (40)$$

$$SS_{tot} = \sum (y - \bar{y})^2 \quad (41)$$

Being y the real time case from the data set of the experiment, \bar{y} the mean value of the vector y and f the reconstruction time vector using n mode combinations.

$$y = \mathcal{C}_y(i, :, k, l) \text{ for a certain } i, k \text{ and } l.$$

$$f(n) \simeq \mathcal{S}_n \times_1 \mathbf{U}^{(1)} \times_2 \mathbf{U}^{(2)} \times_3 \mathbf{U}^{(3)} \times_4 \mathbf{U}^{(4)} \quad (42)$$

Where \mathcal{S}_n is a $3 \times 3 \times 3 \times 3$ tensor whose entries are all zero except for the entries corresponding to the value n , where $n \leftrightarrow (i, j, k, l)$.

This iterative procedure gives as a result the Table 4. Each value of the table represents the value of the coefficient of determination obtained by the contribution of the sum of mode combinations. For instance, the value of the first time case (1, :, 1, 1) corresponding to the fourth column, which is 0.8644, is the value of the coefficient of determination corresponding to the time case reconstruction using the four previous combination of modes, that is, using the mode combination (1, 1, 1, 1), (1, 2, 1, 2), (2, 1, 1, 2) and (2, 2, 1, 1). In addition, the last column shows the comparison of the tensor entries previously seen in Table 3. The time cases selected to show the coefficient of determination were chosen randomly.

n	Time vector cases						$\mathcal{S}_{i,j,k,l}^2 / \sum \mathcal{S}_{i,j,k,l}^2$ (%)
	(1,:,1,1)	(1,:,1,2)	(1,:,2,1)	(2,:,1,1)	(2,:,1,2)	(2,:,2,2)	
1 _(1,1,1,1)	0.6543	0.8300	0.6398	0.7971	0.8717	0.8799	93.82
2 _(1,2,1,2)	0.8241	0.9686	0.2915	0.9549	0.9824	0.9948	3.49
3 _(2,1,1,2)	0.8711	0.9686	0.3199	0.9577	0.9828	0.9952	0.43
4 _(2,2,1,1)	0.8644	0.9633	0.3981	0.9551	0.9803	0.9822	0.37
5 _(1,2,2,1)	0.8801	0.9767	0.3395	0.9551	0.9809	0.9833	0.35
6 _(2,1,1,3)	0.9300	0.9767	0.3186	0.9619	0.9807	0.9831	0.28
7 _(2,2,1,1)	0.9360	0.9848	0.3194	0.9691	0.9881	0.9802	0.19

Table 4: Coefficient of determination as function of time cases and number of mode combinations.

Table 4 shows that the combination of the first two modes is valid for the majority of cases of the tensor \mathcal{C}_y , for instance the case (2,:,2,2) shown in Fig.16a. Note that four out of six random cases are clearly defined with only the use of the first two mode combination to performed the reconstruction. This means that *comparison method* is a valid method to extract the global behavior of the different parameters present in the experiment.

Moreover, other interest information that can be extracted from Table 4 is that there are some cases, for instance (1,:,1,1) shown in Fig.16b, that need more than these two mode combination to be clearly defined.

Furthermore, the case (1,:,2,1), shown in Fig. 16c, clearly shows that the previous method is not valid for this particular case. This concludes that the *comparison method* is not valid for all cases. In this instance, a different set of mode combinations must be used to be able to define this case.

Summarizing, the *comparison method* is a good method to extract the global behavior of each variable of the experiment. Nonetheless, there are some exceptions:

- Some cases need more mode combination than others to be fully understandable.
- Some cases are not defined with the combination proposed by the *comparison method*. In these cases, another different set of modes must be used to define that cases.

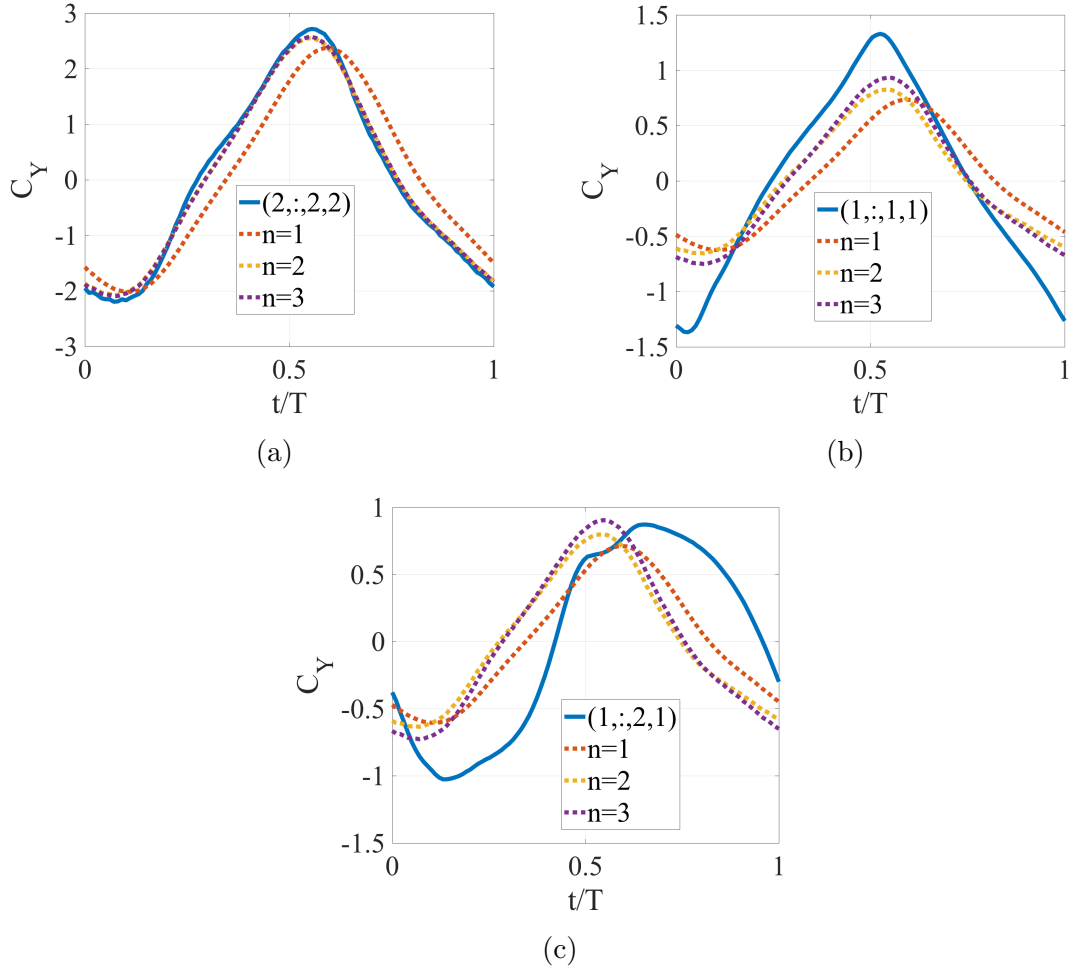


Figure 16: (a) Reconstruction of $C_Y(2, :, 2, 2)$; (b) Reconstruction of $C_Y(1, :, 1, 1)$; (c) Reconstruction of $C_Y(1, :, 2, 1)$

Once shown the validity of the *comparison method*, Table 3 shows that the effect of θ_0 and θ_m on C_Y is clearly defined with the first mode of each parameter as seen in the experimental cases. On the other hand, the effect of time as well as the *Strouhal number* effect on the force coefficient is a combination of the first two modes of each parameter, specially in the case of the influence of time, where shift appears.

With this information, a simple approximate mathematical model can be extracted taking into consideration a shift of 90° and that the θ_m parameter does not have any relevant effect on C_Y . The functions f_1 , f_2 and f_3 can be approximated to be linear.

$$C_Y = f_1(\theta_0) \left[f_2(St) \sin(2\pi ft + \phi) + f_3(St) \sin(2\pi ft + \phi + \frac{\pi}{2}) \right] \quad (43)$$

5.2 Parametric study of C_X

The results of *comparison method* for the case of C_X are displayed in Table 5.

n	(i, j, k, l)	$\mathcal{S}_{i,j,k,l}^2 / \sum \mathcal{S}_{i,j,k,l}^2 (\%)$
1	(1,1,1,1)	78.46
2	(1,2,1,2)	6.18
3	(1,2,2,1)	4.84
4	(2,3,1,1)	2.64
5	(2,3,1,2)	0.64
6	(3,3,1,1)	0.58
7	(3,2,3,1)	0.56

Table 5: Leading mode combinations of C_X according to the *comparison method*.

In the case of the C_Y , the *comparison method* gave as a result that the first two mode combinations were enough to fully describe the behavior of the average of the whole ensemble. Nevertheless, for the case of C_X , it seems that is needed at least the first four mode combinations to describe the behavior of the system. This translates into a more complex results because the whole ensemble is influenced by a larger number of modes.

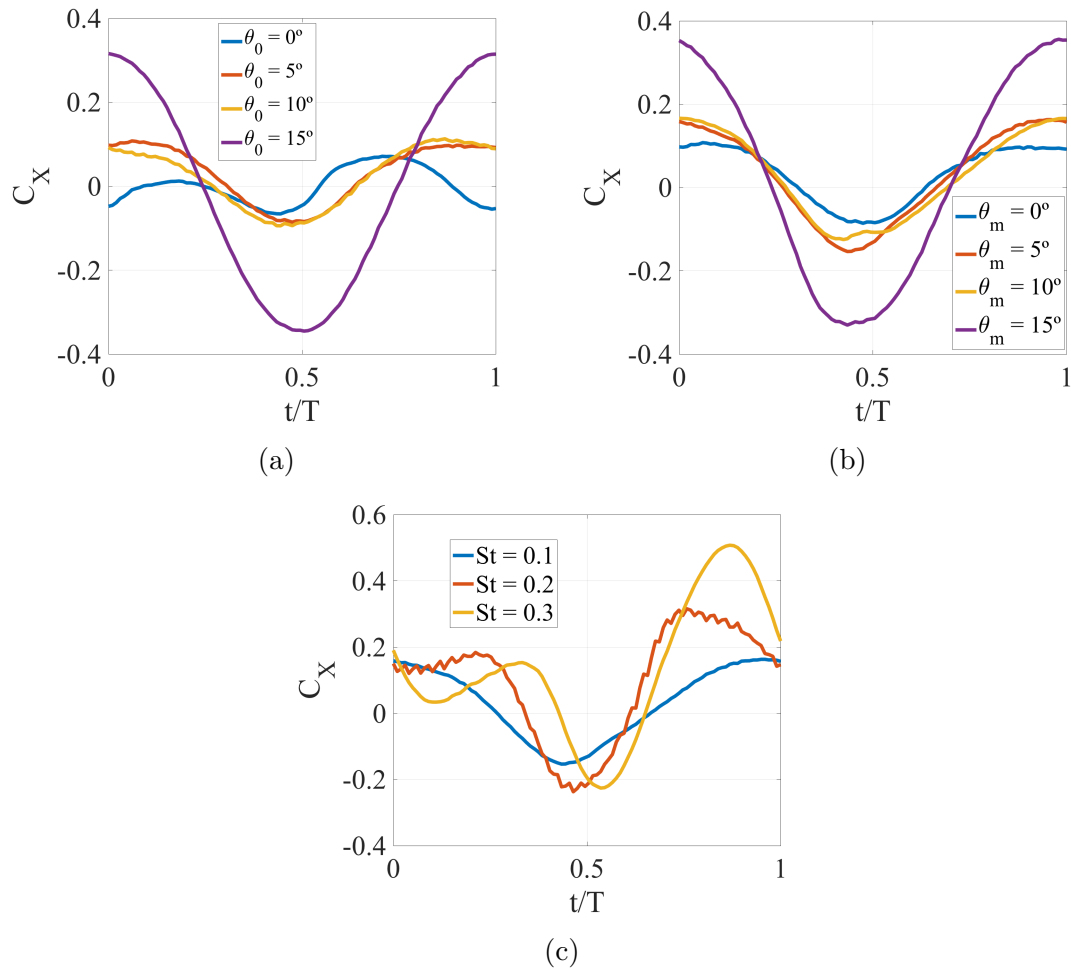


Figure 17: (a) θ_0 effect on C_X with $\theta_m = 0^\circ$ and $St = 0.1$; (b) θ_m effect on C_X with $\theta_0 = 5^\circ$ and $St = 0.1$; (c) St effect on C_X with $\theta_0 = 5^\circ$ and $\theta_m = 5^\circ$.

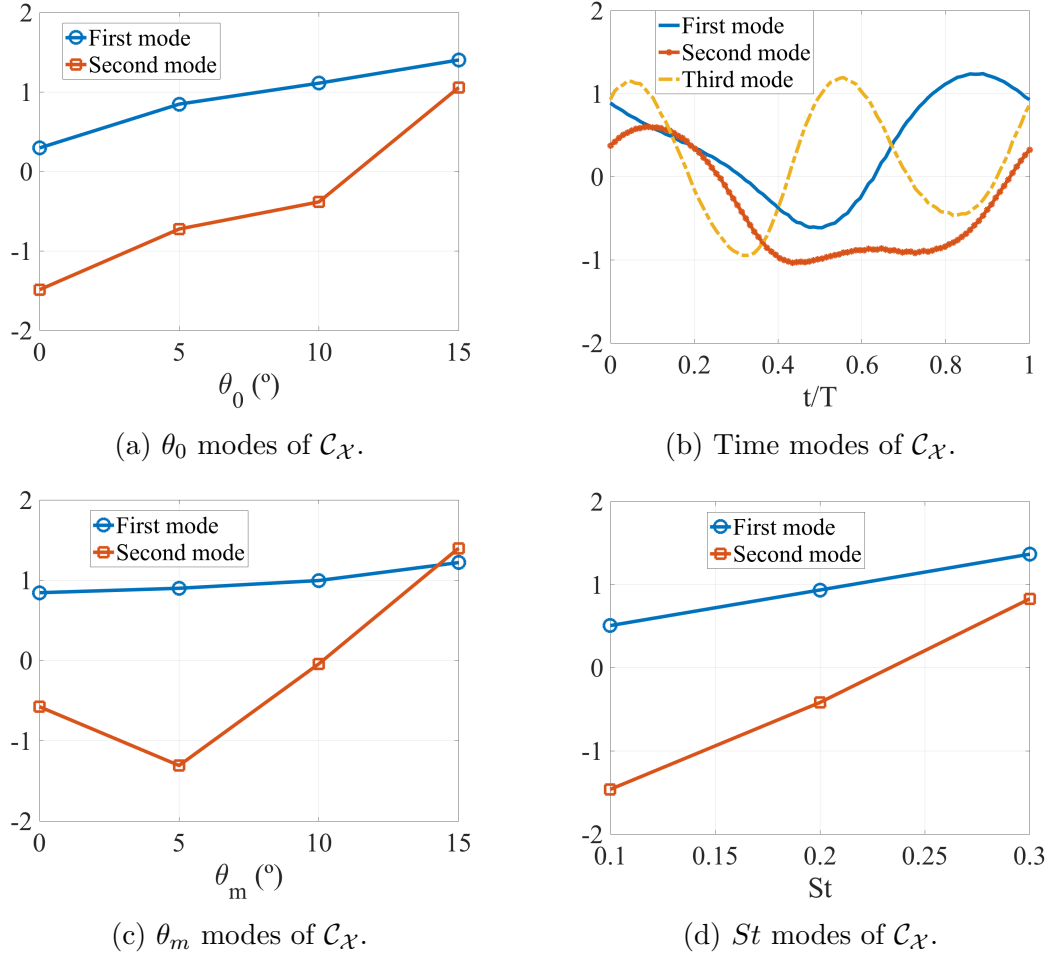
Figure 18: Most important modes combination of C_X .

Fig. 18 shows the most relevant modes of the C_X tensor according to the *comparison method* seen in Table 5.

First of all, it should stand out that the combination of time modes (Fig. 18b) leads to the actual shape of the cases as function of time. It can be seen a little shift recurrent in all the cases due to the combination of the first three time modes, similar to the case of C_Y .

The overall effect of the θ_0 modes (Fig. 18a) for the set of cases is that increasing θ_0 , the amplitude of C_X increases as well, as seen in Fig. 17a.

The same happens with the effect of the *Strouhal number*. The St modes (Fig. 18d) can be approximated accurately to a linear function with a slope of 2.478 for the first St mode and a slope of 6.615 for the second mode. This means that the amplitude of C_X increases as the *Strouhal number* value increases as shown in Fig. 17c.

n	Time vector cases						
	(1,:,1,1)	(1,:,1,2)	(1,:,2,1)	(2,:,1,1)	(2,:,1,2)	(2,:,2,2)	(3,:,3,3)
1 _(1,1,1,1)	-0.0353	0.0760	0.0281	0.8457	0.4967	0.8078	0.9187
2 _(1,2,1,2)	-0.4595	0.0803	-0.3886	0.5863	0.4585	0.7917	0.9548
3 _(1,2,2,1)	-0.3271	0.0734	-0.1188	0.7792	0.5030	0.7665	0.9549
4 _(2,3,1,1)	-0.6259	0.2888	-0.6943	0.7178	0.5720	0.7905	0.9407
5 _(2,3,1,2)	-0.7971	0.3757	-0.8666	0.6311	0.7167	0.8748	0.9487
6 _(3,3,1,1)	-1.3731	0.3673	-0.7388	0.6013	0.7130	0.8670	0.9473

Table 6: Coefficient of determination as function of time cases and number of mode combinations.

On the other hand, the effect of θ_m modes (Fig. 18b) is that as increasing the value of θ_m the amplitude of C_X grows and the C_X curve losses its periodicity. This phenomena can be seen in Fig. 17b.

Table 6 shows the values of the coefficient of determination for the case of C_X obtained in the same way that Table 4.

It can be seen that there are some cases that are clearly defined with just two mode combinations like the case (3, :, 3, 3) depicted in Fig. 19a. Besides, there are other cases that need extra mode combinations to be clearly defined, for instance the case (1, :, 1, 2) shown in Fig. 19b. But, on top of this, there are some other cases with a negative coefficient of determination, which means that the mode combinations from which the reconstruction is done, cannot be used to describe the behaviour of that case at all. In those cases, another completely set of combination of modes must be used to defined them.

In the C_Y case, the coefficient of determination showed the validity of the comparison method, but there were some exceptions. These exceptions are accentuated in the case of C_X . In other words, the *comparison method* is not completely valid to select the most important mode combination for C_X . Even so, it provides good results in general, as seen before with the plots of each mode.

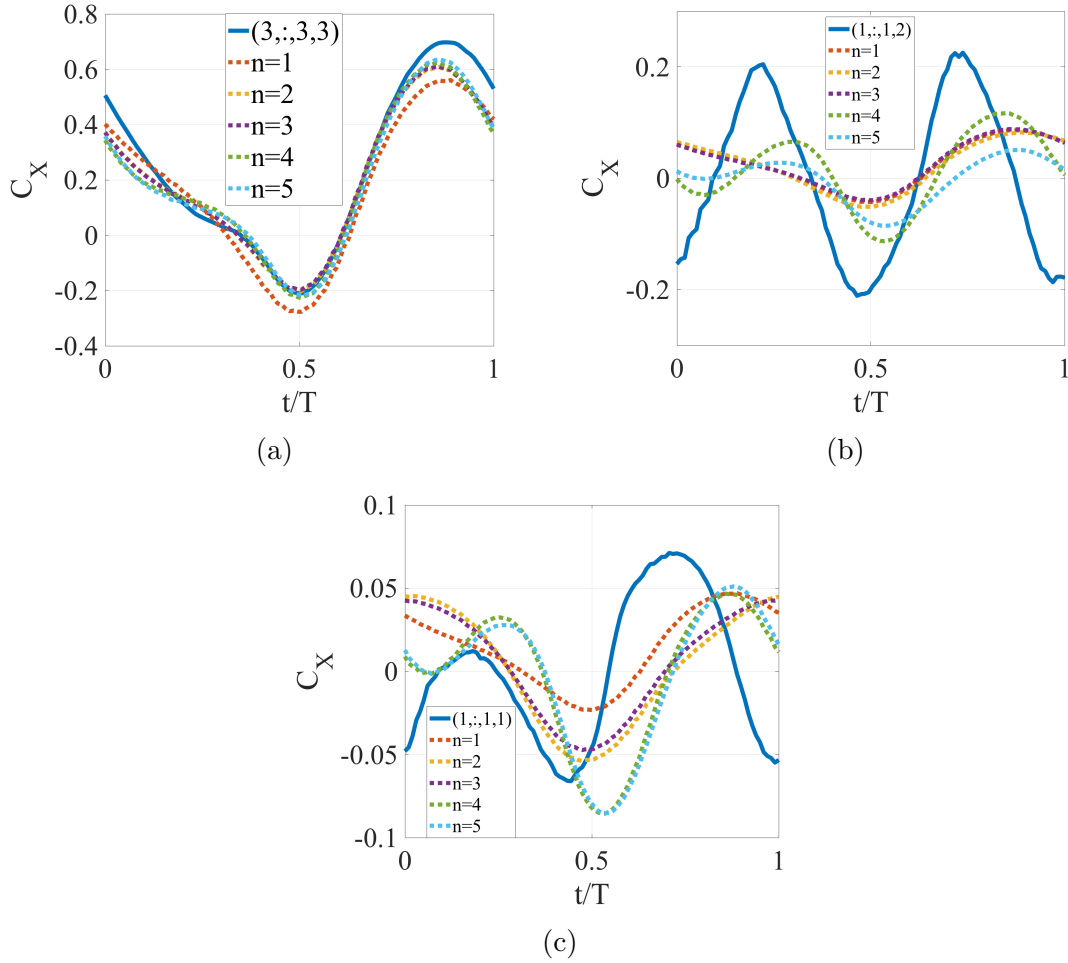


Figure 19: (a) Reconstruction of C_X $(3, :, 3, 3)$; (b) C_X $(1, :, 1, 2)$; (c) C_X $(1, :, 1, 1)$ with n mode combinations.

Some of the reasons why the *comparison method* is not a feasible method to select the most relevant mode combinations for majority of cases of C_X could be:

- The force in the x -direction of a flapping wing is much more complex than the force in y -direction.
- There may exist some physical phenomena that could change C_X abruptly while changing some of the parameters and cannot be evaluated with the first mode combinations obtained with the *comparison method*, e.g., sudden separation of the LEV for a certain value of St . The *comparison method* takes into account all the data set as equal and cannot predict sudden physical behaviors.

- The data set for the C_X is not as accurate as the one of C_Y . The data set of C_X should have more sample points and a higher *signal-to-noise* ratio. The latter factor plays an important role in modal decomposition problems. The magnitude of the forces in *y-direction* are much larger than in *x-direction*. However, the measure instruments used by Carrillo [2] were the same, so the magnitude of the noise for the case of C_Y and C_X is similar. With a similar level of noise but with a less signal intensity, the *signal-to-noise* ratio of C_X is much smaller than for the case of C_Y . This larger level of noise could accentuate the error produce by the *comparison method* at extracting the most important mode combinations.

6 Discussion and summary

This section discusses the results from a literature point of view. Finally, the final conclusions of the thesis are summarized.

In order to ease the reading of the discussion section, Table 7 summarizes the effect of each parameter studied on the amplitude of both force coefficients.

	Increasing θ_0	Increasing θ_0	Increasing St
C_Y	Decreases (linear)	Constant (small positive slope)	Increases (linear)
C_X	Increases	Increases	Increases (linear)

Table 7: Summary of the effect of each parameter on the amplitude of C_Y and C_X according to the modal decomposition results.

6.1 Effect of pitching amplitude θ_0 and mean pitch angle θ_m

After an extensive literature review, the effect of θ_0 and θ_m parameter on the fluctuating part of the force magnitude is difficult to predict and there is no a common agreement that explains the effect of θ_0 on the magnitude. Nevertheless, in the thesis of Carrillo [2], the effective angle of attack is studied varying θ_0 and θ_m parameters. These variations are depicted in Fig. 20a and 20b. As seen in Eq. 30, the effective angle of attack depends on the pitching motion $\theta(t)$ and the first derivative of the heave motion $\dot{h}(t)$. Besides, assuming that $C_D \ll C_L$, C_Y of Eq. 36 can be written as:

$$C_Y \approx C_L \cos \theta \quad (44)$$

Where C_L can be approximated to:

$$C_L \approx 2\pi\alpha_{eff} \quad (45)$$

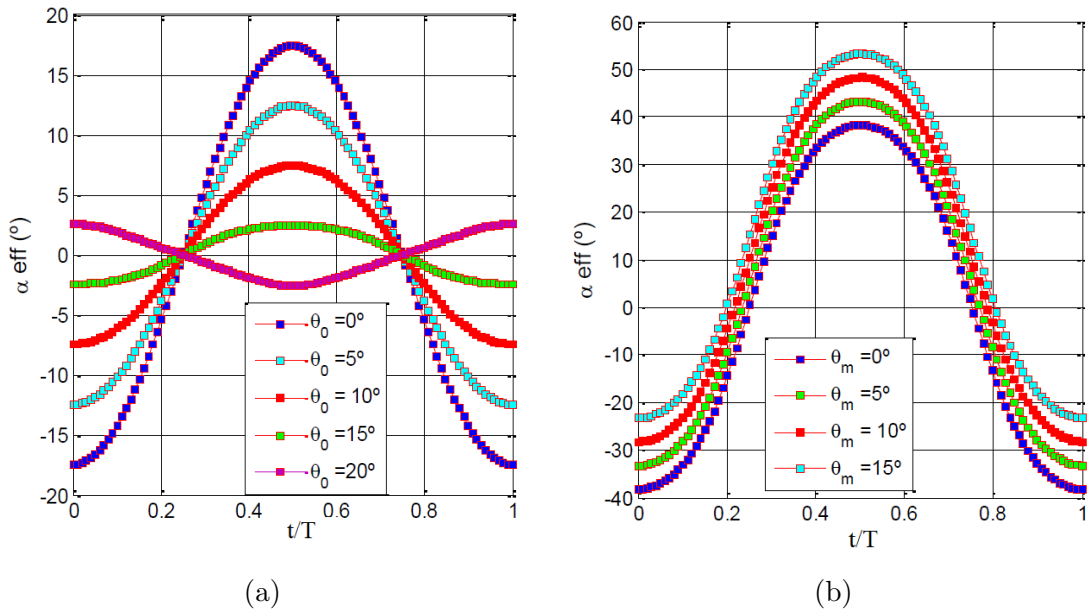


Figure 20: Variation of the effective angle of attack (α_{eff}) with θ_0 (a) and θ_m (b). Adopted from [2].

Then, Fig. 20a shows a decrease of the effective angle of attack as θ_0 increases. This translates into a decrease of the amplitude of C_Y as it can be seen in the results obtained (Fig. 14a). Moreover, it should be pointed out that the linear effect of θ_0 on C_Y may be only applicable for the specified set of parameters that have been established, this is, the phase angle between pitching and plunging is 90° ($\phi = 90^\circ$) and $h_0/c = 1$ among others.

On the other hand, Fig. 20b depicts that the variation of the angle of attack with θ_m has much less intensity than for the case of θ_0 . In addition, it can be seen a little increase of the effective angle of attack as θ_m increases. This effect is seen in Fig. 14c where the θ_m function has a little positive slope.

6.2 Effect of the *Strouhal number*

The fact that both force coefficients amplitude (C_Y and C_X) increases with an increase of the *Strouhal number* is simple to explain. An increase in the *Strouhal number* means an increase in the heave motion frequency (as seen in Eq. 31) which leads to an increase in lift force but to an increase in drag too. Additionally, Kang et al. [63] observed that at higher values of *Strouhal number* the LEV was formed at later times, which it can be translated to a larger force magnitudes. Besides, Lai & Platzer [64]

discovered that the wake produced by pure heave motion can be described as function of the *Strouhal number* up to a limit of $St = 0.6$ where the wake becomes asymmetric and difficult to predict. Jones, Dohring & Platzer [57] developed a model to predict the wake structure of a flapping airfoil under pitching and plunging motions. They discovered that for low values of St ($St \approx 0.06$) the viscous effect becomes dominant. Additionally, an experiment taken by Koochesfahani [65] showed what Triantafyllou et al. [58] hypothesized in 1993, that the optimal efficiency of a flapping airfoil is obtained at the frequency of maximum spatial amplification of the wake, which lies into a range of $0.25 \leq St \leq 0.35$.

6.3 Summary

With the experimental data obtained by Carrillo [2], the effect of each parameter was seen. However, it was impossible to predict the actual mathematical function that governs the effect of each parameter. After doing the modal decomposition, it can be known deeply how each parameter affects the force coefficient by approximating this effect into a mathematical function. For instance, thanks to the modal decomposition it can be concluded that the effect of θ_0 parameter on C_Y is linear as well as the effect of the *Strouhal number*. Nonetheless, this conclusion must be treated carefully. The linear behavior appears under the specific assumption of certain parameters like a low Reynolds, a phase angle of 90° or $h_0/c = 1$ among others.

After this work, the modal decomposition has shown that it is a very powerful method to obtain information about a complex system like flapping wings, without the necessity of entering into too much detail in the fluid mechanics field. Modal decomposition method has been able to not only extract the effect of each parameter but to obtain an approximation function of that effect.

With the coefficient of determination procedure, the *comparison method* was shown to be a valid method to extract the most relevant mode combinations. However, the main limitation of MLSVD is that not all cases are well defined with the same mode combinations. Even so, it provides good results for the majority of cases.

Moreover, the *Tucker Decomposition* has allowed to expand to more than two dimensions the *Singular Value Decomposition* method to a very complex field like fluid mechanics.

Finally, although the tensor decomposition is the best method to see the influence of each parameter, it does not provide any information about the physical explanation of the system. In other words, it is an insufficient method to describe complex behaviors such as the leading and trailing edge vortexes, wake formation or dynamic stall.

In a nutshell, MLSVD allows to analyze multivariable data and see how each parameter affects to the system without the need of using complex models that try to simulate the physics behind a fluid mechanics problem.

7 Future work

With this work, the application of modal decomposition for more than two parameters in a fluid mechanics problem has been shown. The *N-way principal component analysis* can be used to obtain the most relevant modes of each parameter to any fluid mechanics problem, or even for any problem involving a large number of variables out of the scope of fluid mechanics. For instance, one possible application would be to apply the multilinear modal decomposition to problems that involves velocity fields, such as the flow over a bluff body in order to see the main modes that govern the vorticity formation. However, a velocity field instead of force values results in a much more difficult problem since it involves a vectorial field instead of a scalar such as a force coefficient.

Moreover, this work should be extended with a data set with more sample points and by studying the effect of the rest of parameters not considered in this paper, such as the *Reynolds number*, the chord, the camber of the airfoil, the heave amplitude, or the phase angle between heave and pitching motions among others. This extended study could be used in order to see more effects in case of interaction between parameters and validate the results obtained in this thesis.

Last but not least, the so-called *comparison method* of this paper has shown its effectiveness in ordering the most relevant mode combinations. Nevertheless, this method has some exceptions, as seen in the case of C_X . In this way, the *comparison method* could be improved to increase its efficiency.

References

- [1] N. Vervliet et al. *Tensorlab 3.0*. Available online. Mar. 2016. URL: <https://www.tensorlab.net>.
- [2] María del Mar Carrillo. “Force generation in flapping wings: A parametric study”. In: *Universidad Carlos III de Madrid* (2017).
- [3] Irving John Good. “Some applications of the singular decomposition of a matrix”. In: *Technometrics* 11.4 (1969), pp. 823–831.
- [4] Sergio LM Freire and Tad J Ulrych. “Application of singular value decomposition to vertical seismic profiling”. In: *Geophysics* 53.6 (1988), pp. 778–785.
- [5] Afsaneh Safavi and Hamid Abdollahi. “Thermodynamic characterization of weak association equilibria accompanied with spectral overlapping by a SVD-based chemometric method”. In: *Talanta* 53.5 (2001), pp. 1001–1007.
- [6] James B Clarage et al. “A sampling problem in molecular dynamics simulations of macromolecules.” In: *Proceedings of the National Academy of Sciences* 92.8 (1995), pp. 3288–3292.
- [7] Daniel P Berrar, Werner Dubitzky, Martin Granzow, et al. *A practical approach to microarray data analysis*. Springer, 2003, pp. 91–109.
- [8] John Leask Lumley. “The structure of inhomogeneous turbulent flows”. In: *Atmospheric turbulence and radio wave propagation* (1967).
- [9] Lawrence Sirovich. “Turbulence and the dynamics of coherent structures. I. Coherent structures”. In: *Quarterly of applied mathematics* 45.3 (1987), pp. 561–571.
- [10] Gal Berkooz, Philip Holmes, and John L Lumley. “The proper orthogonal decomposition in the analysis of turbulent flows”. In: *Annual review of fluid mechanics* 25.1 (1993), pp. 539–575.
- [11] Xinzhong Chen and Ahsan Kareem. “Proper orthogonal decomposition-based modeling, analysis, and simulation of dynamic wind load effects on structures”. In: *Journal of Engineering Mechanics* 131.4 (2005), pp. 325–339.
- [12] S Bernero and HE Fiedler. “Application of particle image velocimetry and proper orthogonal decomposition to the study of a jet in a counterflow”. In: *Experiments in Fluids* 29.1 (2000), S274–S281.
- [13] TT Bui, M Damodaran, and K Wilcox. “Proper orthogonal decomposition extensions for parametric applications in transonic aerodynamics (AIAA Paper 2003-4213)”. In: *Proceedings of the 15th AIAA Computational Fluid Dynamics Conference*. 2003.

- [14] BI Epureanu, KC Hall, and EH Dowell. “Reduced-order models of unsteady viscous flows in turbomachinery using viscous–inviscid coupling”. In: *Journal of Fluids and Structures* 15.2 (2001), pp. 255–273.
- [15] Hung V Ly and Hien T Tran. “Modeling and control of physical processes using proper orthogonal decomposition”. In: *Mathematical and computer modelling* 33.1-3 (2001), pp. 223–236.
- [16] Göran Bergqvist and Erik G Larsson. “The higher-order singular value decomposition: Theory and an application [lecture notes]”. In: *IEEE Signal Processing Magazine* 27.3 (2010), pp. 151–154.
- [17] Ledyard R Tucker and Samuel Messick. “An individual differences model for multidimensional scaling”. In: *Psychometrika* 28.4 (1963), pp. 333–367.
- [18] Ledyard R Tucker. “Some mathematical notes on three-mode factor analysis”. In: *Psychometrika* 31.3 (1966), pp. 279–311.
- [19] Lieven De Lathauwer, Bart De Moor, and Joos Vandewalle. “A multilinear singular value decomposition”. In: *SIAM journal on Matrix Analysis and Applications* 21.4 (2000), pp. 1253–1278.
- [20] Arie Kapteyn, Heinz Neudecker, and Tom Wansbeek. “An approach to n-mode components analysis”. In: *Psychometrika* 51.2 (1986), pp. 269–275.
- [21] Frank L Hitchcock. “The expression of a tensor or a polyadic as a sum of products”. In: *Journal of Mathematics and Physics* 6.1-4 (1927), pp. 164–189.
- [22] Raymond B Cattell. ““Parallel proportional profiles” and other principles for determining the choice of factors by rotation”. In: *Psychometrika* 9.4 (1944), pp. 267–283.
- [23] J Douglas Carroll, Sandra Pruzansky, and Joseph B Kruskal. “CANDELINC: A general approach to multidimensional analysis of many-way arrays with linear constraints on parameters”. In: *Psychometrika* 45.1 (1980), pp. 3–24.
- [24] Richard A Harshman. “Foundations of the PARAFAC procedure: Models and conditions for an “explanatory” multimodal factor analysis”. In: (1970).
- [25] Henk AL Kiers. “Towards a standardized notation and terminology in multi-way analysis”. In: *Journal of Chemometrics: A Journal of the Chemometrics Society* 14.3 (2000), pp. 105–122.
- [26] Pieter M Kroonenberg and Jan De Leeuw. “Principal component analysis of three-mode data by means of alternating least squares algorithms”. In: *Psychometrika* 45.1 (1980), pp. 69–97.
- [27] Claus A Andersson and Rene Henrion. “A general algorithm for obtaining simple structure of core arrays in N-way PCA with application to fluorometric data”. In: *Computational statistics & data analysis* 31.3 (1999), pp. 255–278.

- [28] R Henrion et al. “Three-way principal components analysis for fluorescence spectroscopic classification of algae species”. In: *Fresenius’ journal of analytical chemistry* 357.5 (1997), pp. 522–526.
- [29] Takashi Murakami, Jos MF Ten Berge, and Henk AL Kiers. “A case of extreme simplicity of the core matrix in three-mode principal components analysis”. In: *Psychometrika* 63.3 (1998), pp. 255–261.
- [30] Henk AL Kiers, Jos MF Ten Berge, and Roberto Rocci. “Uniqueness of three-mode factor models with sparse cores: The $3 \times 3 \times 3$ case”. In: *Psychometrika* 62.3 (1997), pp. 349–374.
- [31] Ajit Rajwade, Anand Rangarajan, and Arunava Banerjee. “Image denoising using the higher order singular value decomposition”. In: *IEEE Transactions on Pattern Analysis and Machine Intelligence* 35.4 (2013), pp. 849–862.
- [32] Kunihiko Taira et al. “Modal analysis of fluid flows: An overview”. In: *Aiaa Journal* (2017), pp. 4013–4041.
- [33] Tamara G Kolda and Brett W Bader. “Tensor decompositions and applications”. In: *SIAM review* 51.3 (2009), pp. 455–500.
- [34] Lloyd N Trefethen and David Bau III. *Numerical linear algebra*. Vol. 50. Siam, 1997.
- [35] Henk AL Kiers and Albert Der Kinderen. “A fast method for choosing the numbers of components in Tucker3 analysis”. In: *British Journal of Mathematical and Statistical Psychology* 56.1 (2003), pp. 119–125.
- [36] Michael Smith and Michael Smith. “Reinstating inquiry into mechanized flapping-wing flight-Realizing the integrity of the ornithopter”. In: *35th Aerospace Sciences Meeting and Exhibit*. 1997, p. 533.
- [37] Michael S Triantafyllou and George S Triantafyllou. “An efficient swimming machine”. In: *Scientific american* 272.3 (1995), pp. 64–70.
- [38] Wei Shyy et al. *An introduction to flapping wing aerodynamics*. Vol. 37. Cambridge University Press, 2013.
- [39] Douglas A Read, FS Hover, and MS Triantafyllou. “Forces on oscillating foils for propulsion and maneuvering”. In: *Journal of Fluids and Structures* 17.1 (2003), pp. 163–183.
- [40] Leonardo Da Vinci. “Codex on the flight of birds”. In: (1505).
- [41] Richard Knoller. “Die Gesetzedes Luftwiderstandes”. In: *Flug-und Motortech-nik (Wien)* 3.21 (1909), pp. 1–7.
- [42] Albert Betz. “Ein Beitrag zur Erklarung Segelfluges”. In: *Z Flugtech Motor-luftschiffahrt* 3 (1912), pp. 269–272.
- [43] Richard Katzmayr. “Effect of periodic changes of angle of attack on behavior of airfoils”. In: (1922).

- [44] Shatswell Ober. “Note on the Katzmayer effect on airfoil drag”. In: (1925).
- [45] Theodore Theodorsen. “General theory of aerodynamic instability and the mechanism of flutter”. In: *NACA Technical Report* 496 (1935).
- [46] IE Garrick. “Propulsion of a flapping and oscillating airfoil (NACA (4), R. 567)”. In: *Zbl62* 1583 (1936).
- [47] Theodore Theodorsen. “General theory of aerodynamic instability and the mechanism of flutter”. In: (1949).
- [48] Peter Freymuth. “Propulsive vortical signature of plunging and pitching airfoils”. In: *AIAA journal* 26.7 (1988), pp. 881–883.
- [49] Charles P Ellington et al. “Leading-edge vortices in insect flight”. In: *Nature* 384.6610 (1996), p. 626.
- [50] Knut Streitlien, George S Triantafyllou, and Michael S Triantafyllou. “Efficient foil propulsion through vortex control”. In: *Aiaa journal* 34.11 (1996), pp. 2315–2319.
- [51] JM Anderson et al. “Oscillating foils of high propulsive efficiency”. In: *Journal of Fluid Mechanics* 360 (1998), pp. 41–72.
- [52] Gregory C Lewin and Hossein Haj-Hariri. “Modelling thrust generation of a two-dimensional heaving airfoil in a viscous flow”. In: *Journal of Fluid Mechanics* 492 (2003), pp. 339–362.
- [53] Michael H Dickinson, Fritz-Olaf Lehmann, and Sanjay P Sane. “Wing rotation and the aerodynamic basis of insect flight”. In: *Science* 284.5422 (1999), pp. 1954–1960.
- [54] James M Birch and Michael H Dickinson. “Spanwise flow and the attachment of the leading-edge vortex on insect wings”. In: *Nature* 412.6848 (2001), p. 729.
- [55] Kenneth C Hall and Steven R Hall. “Minimum induced power requirements for flapping flight”. In: *Journal of Fluid Mechanics* 323 (1996), pp. 285–315.
- [56] Kenneth C Hall, Steven A Pigott, and Steven R Hall. “Power requirements for large-amplitude flapping flight”. In: *Journal of Aircraft* 35.3 (1998), pp. 352–361.
- [57] KD Jones, CM Dohring, and MF Platzer. “Experimental and computational investigation of the Knoller-Betz effect”. In: *AIAA journal* 36.7 (1998), pp. 1240–1246.
- [58] George S Triantafyllou, MS Triantafyllou, and MA Grosenbaugh. “Optimal thrust development in oscillating foils with application to fish propulsion”. In: *Journal of Fluids and Structures* 7.2 (1993), pp. 205–224.
- [59] Haecheon Choi, Woo-Pyung Jeon, and Jinsung Kim. “Control of flow over a bluff body”. In: *Annu. Rev. Fluid Mech.* 40 (2008), pp. 113–139.

- [60] Sewall Wright. “Correlation and causation”. In: *Journal of agricultural research* 20.7 (1921), pp. 557–585.
- [61] Jay L Devore. *Probability and Statistics for Engineering and the Sciences*. Cengage learning, 2011.
- [62] A Colin Cameron and Frank AG Windmeijer. “An R-squared measure of goodness of fit for some common nonlinear regression models”. In: *Journal of econometrics* 77.2 (1997), pp. 329–342.
- [63] Chang-kwon Kang et al. “Fluid dynamics of pitching and plunging airfoils of Reynolds number between 1×10^4 and 6×10^4 ”. In: *47th AIAA Aerospace Sciences Meeting including The New Horizons Forum and Aerospace Exposition*. 2009, p. 536.
- [64] JC S. Lai and MF Platzer. “Jet characteristics of a plunging airfoil”. In: *AIAA journal* 37.12 (1999), pp. 1529–1537.
- [65] Manoochehr M Koochesfahani. “Vortical patterns in the wake of an oscillating airfoil”. In: *AIAA journal* 27.9 (1989), pp. 1200–1205.